令和 5 年度

Doctoral Dissertation

博士学位論文

Electron spin dynamics of dilute nitride GaNAs quantum well–InAs quantum dots tunnel-coupled nanostructures

希薄窒化 GaNAs 量子井戸—InAs 量子ドット

トンネル結合ナノ構造の電子スピンダイナミクス

Graduate School of Information Science and Technology

Hokkaido University

北海道大学大学院 情報科学院

Shino Sato

佐藤　紫乃

Contents

Acknowledgement

I would like to express my appreciation to my thesis advisor Professor Akihiro Murayama for his valuable advice and discussions throughout the entire duration of my scientific research.

I would also like to thank to my thesis committee: Professor Junichi Motohisa and Professor Kazuhisa Sueoka, for their comments to improve my thesis.

I am also particularly grateful to Associate Professor Satoshi Hiura, Mr. Junichi Takayama and Associate Professor Hirotake Sugawara for them continuous support and thoughtful guidance, advice, and technical support on my study.

And I would thank all the members in the Laboratory of Electronic and Photonic Materials who helped me with active participation in daily experiments and discussions.

This work was supported by JSPS Grant-in-Aid for JSPS Research Fellow Grant Number JP21J20076.

Chapter1. Introduction

1.1 Background

In recent years, the volume of processed information has rapidly increased due to the expanding use of cloud computing and artificial intelligence. Given such rising data volumes, reducing power consumption for information processing has become imperative. Optical wiring technology based on photon–electron spin information conversion is garnering interest as a component for ultra-low power information processing platforms. In semiconductor-based photon–electron spin information conversion, electron spin information is converted into light polarization information via luminescence recombination between electrons and holes without energy consumption [1]. In addition, the power consumption of optical wiring platforms is low, as these systems utilize light for signal wiring between electronic circuits and systems, thereby preventing the heat loss that is generally associated with electrical wiring.

In photon–electron spin information conversion, the information is stored as the spin polarization of the electron spins and converted into the circular polarization of the emitted light. The circularly polarization degree (CPD) can be described as

$$CPD\ (\%) = \frac{I_{\sigma+} - I_{\sigma-}}{I_{\sigma+} + I_{\sigma-}} \times 100 \approx \frac{N_{\sigma+} - N_{\sigma-}}{N_{\sigma+} + N_{\sigma-}} \times 100, \qquad (1-1)$$

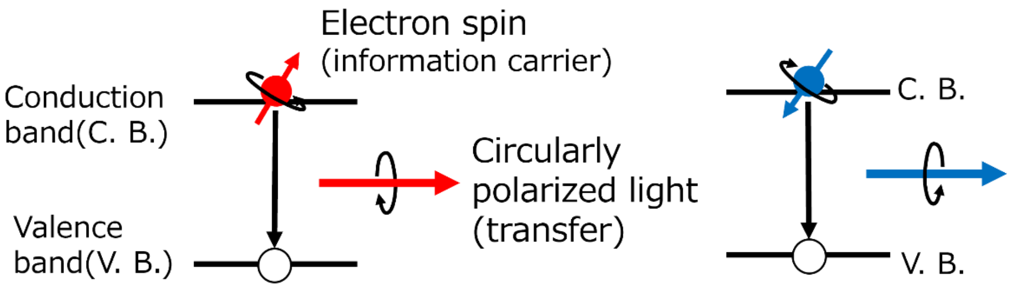

Figure 1-1. Schematic illustration of photon-electron spin information conversion.

where $I_{\sigma+}(I_{\sigma-})$ denotes the emission intensity associated with electrons with majority (minority) spin and $N_{\sigma+}(N_{\sigma-})$ denotes the number of electrons with majority (minority) spin. The relaxation time of hole spin is extremely fast [2, 3, 4]; hence, the CPD reflects the spin polarization degree of electron spins. To transfer the stored information correctly, a high CPD must be maintained during emission, i.e., the spin polarization of the electron spin polarization must be kept high.

To realize spin-functional optical devices, which serve as light sources for optical wiring through the conversion of photon–electron spin information, it is imperative to identify materials and structures capable of both preserving electron spin information for extended durations and efficiently converting electron spin into light. In addressing the former consideration, ferromagnetic metals are extensively employed for electron spin storage due to their proficiency in maintaining spin information over time. However, it is noteworthy that these materials lack the capability to effectually convert electron spin into light. In contrast, current applications leverage bulk semiconductors and semiconductor quantum wells (QWs) for light-emitting devices, showcasing the ability to convert electron spin into light. Nonetheless, a notable limitation persists, as these materials fail to conserve electron spin information for prolonged periods. Consequently, the pursuit of materials and structures that can simultaneously fulfill both requirements has been a focal point of research endeavors.

1.2 Spin relaxation mechanism in semiconductor

The three typical electron-spin relaxation mechanisms in semiconductor bulk [5] are the D'yakonov–Perel' (DP), Elliot–Yafet (EY), and Bir–Aronov–Pikus (BAP) mechanisms.

1.2.1 D'yakonov–Perel' mechanism

The DP mechanism [6, 7, 8] is caused by the effective magnetic field resulting from the spin-orbit interaction. In an effective magnetic field, the moving electron spins undergo precession motion. Electrons are scattered by impurities and defects, which change their momentum (k vector), and the k-dependent effective magnetic field causes spin relaxation. The spin relaxation time caused by DP mechanism, τ_s^{DP}, is proportional to inverse of the temperature, T, and the momentum scattering time, τ_p. In general, at high temperatures, this DP mechanism emerges as the dominant spin relaxation mechanism in the semiconductor bulk.

1.2.2 Elliot-Yafet mechanism

In the EY mechanism [9, 10, 11], the wavefunction of electrons in the conduction band undergoes mixing with the wavefunction of electrons in the valence band due to spin-orbit interactions. This interaction leads to spin inversion, even in instances of spin-independent scattering. Consequently, whenever an electron scatters and undergoes a change in its orbital momentum, the potential for an electron spin flip exists. Impurities, boundaries, and phonons contribute to the inversion of electron spin through spin-orbit interactions. The spin relaxation time, τ_s^{EY}, attributed to the EY mechanism is proportional to the momentum scattering time, τ_p, and bandgap energy, E_g. Notably, materials characterized by a narrower band gap experience faster spin relaxation through the EY mechanism. Additionally, in contrast to the DP mechanism, the spin relaxation time increases proportionally with τ_p.

1.2.3 Bir-Aronov-Pikus mechanism

The BAP mechanism [12, 13] is a spin relaxation mechanism that results from the exchange interaction between electrons and holes. Due to the strong hybridization of heavy and light holes with different angular momenta in the bulk, the spin relaxation time of holes is extremely fast (a few ps [2]). Thus, their spin states are generally unpolarized. Therefore, the electron spin state relaxes when the electrons exchange and interact with the holes. In microstructures such as QD, the electrons and holes are spatially confined to the same location and the electron-hole interaction is strong, so that spin relaxation by the BAP mechanism dominates.

1.3 Semiconductor quantum dot

A significant challenge encountered in the application of semiconductors to spin-functional optical devices lies in the rapid relaxation of electron spin within semiconductor bulk materials. An encouraging solution to address this challenge is found in III-V semiconductor quantum dots (QDs) [14], which stand out as promising candidates for the optically active layer in spin-functional optical devices, such as spin-polarized emitting diode[15-23].

A semiconductor QD is a nanostructure with a typical diameter in the order of tens of nanometers. In our study, self-assembled QDs were cultivated through molecular beam epitaxy (MBE) on a GaAs (100) substrate. Figure 1-2 illustrates a straightforward representation of the self-assembled QD structure and its

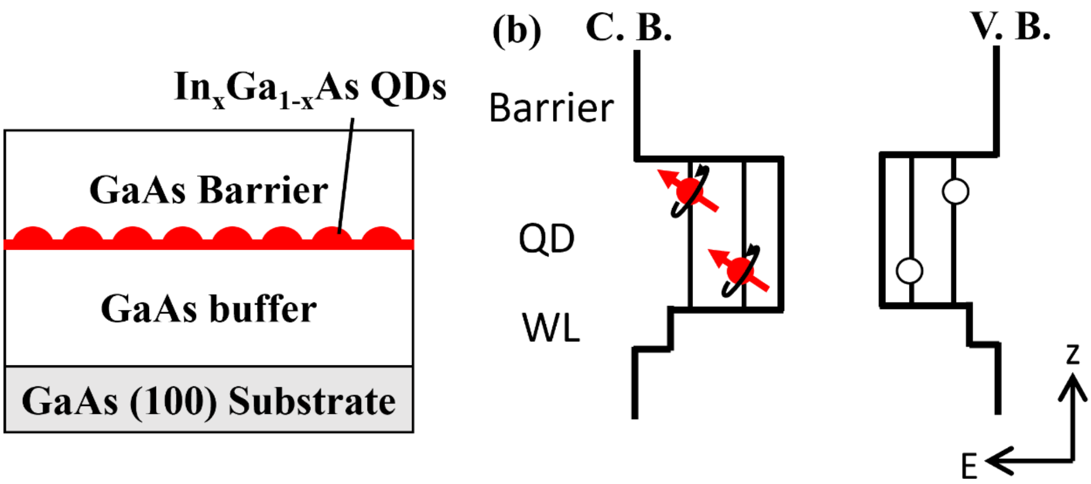

Figure 1-2. Schematic illustration of a simple example of self-assembled QD structure (a) and its energy band structure (b).

corresponding energy band structure. Despite their pyramid- or island-like shapes, QDs exhibit lower energy levels than their surroundings, creating a potential well for electrons and holes, allowing them to be effectively captured.

1.3.1 Optical properties of quantum dot

As previously highlighted, QDs possess lower energy levels compared to their surroundings, creating potential wells for carriers and facilitating their confinement. This spatial confinement of electrons and holes to the same position enhances the radiative recombination probability, leading to effective conversion of electrons into light. Furthermore, a robust three-dimensional quantum confinement effect is induced in the confined electrons [24], resulting in a completely discretized density of states, as illustrated in Figure 1-3. The quantum size effects play a crucial role in this context, as the discretized energy levels of the electrons are inversely proportional to the square of the QD diameter and height. Consequently, smaller QDs exhibit higher energy levels, while larger QDs have lower energy levels [25]. The energy differences between these discrete electronic states can surpass the thermal energy at ambient

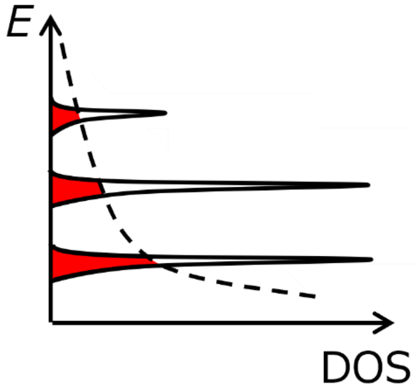

Figure 1-3. Schematic illustration of density of states (DOS) of QDs. The broadening of DOS reflects size or shape distribution of QDs.

temperatures, resulting in minimal variations in the emission wavelength from QDs with temperature changes. This inherent property ensures that the emission wavelength from QDs remains relatively unaffected by temperature, enabling the realization of stable and temperature-independent emission characteristics. laser devices based on QDs have demonstrated significantly smaller temperature variations in optical output characteristics compared to those based on QWs. In particular, Fabry–Perót and distributed feedback lasers based on QDs exhibited almost constant optical output characteristics across a temperature range from –40°C to 100°C [26]. This observation implies that, unlike conventional lasers, QD lasers do not necessitate cooling elements, potentially reducing the power consumption associated with cooling requirements.

1.3.2 Spin properties of semiconductor quantum dot

QDs not only exhibit notable optical properties but also possess spin properties that render them suitable for spin-optical devices [27]. In bulk semiconductors, the dominant DP spin relaxation mechanism involves the scattering of electron spins, moving within the bulk, by impurities and defects. This mechanism leads to a rapid relaxation of the spin polarization degree, rendering it challenging to maintain electron spin information for extended durations. In contrast, within QDs, the three-dimensional quantum confinement effect freezes the momentum of electrons, preventing scattering by impurities and defects. Consequently, the DP spin relaxation mechanism is suppressed, allowing for the conservation of electron spin polarization for a more prolonged duration compared to bulk semiconductors [24, 28-32].

References

[1] F. Meier, and B. Zakharchenya, Optical Orientation, (Elsevier, North-Holland, Amsterdam, 1984).

[2] S. Cortez, O. Krebs, S. Laurent, M. Senes, X. Marie, P. Voisin, R. Ferreira, G. Bastard, J-M. Gérard, and T. Amand, Phys. Rev. Lett. **89**, 207401 (2002).

[3] W. Kauschke, N. Mestres, and M. Cardona, Phys. Rev. B **35**, 3843 (1987).

[4] D. J. Hilton, and C. L. Tang, Phys. Rev. Lett. **89**, 146601 (2002).

[5] I. Zutic, J. Fabian, and S. D. Sarma, Rev. Mod. Phys. **76**, 323 (2004).

[6] M. I. Dyakonov, Spin Physics in Semiconductors, (Springer, Berlin, Heidelberg, 2008).

[7] M. I. Dyakonov, and V. I. Perel, Sov. Phys. JETP **33**, 1053 (1971).

[8] L. Szolnoki, B. Dora, A. Kiss, and F. Simon, Sci, Rep. **7**, 9949 (2017).

[9] R. J. Elliott, Phys, Rev. **96**, 266 (1954).

[10] A. Kiss, L. Szolnoki, and F. Simon, Sci. Rep. **6**, 22706 (2016).

[11] J. -N. Chazalviel, Phys. Rev. **B** 11, 1555 (1975).

[12] A. G. Aronov, G. E. Pikus, and A. N. Titkov, Sov. Phys. JETP **57**, 680 (1983).

[13] G. L. Bir, A. G. Aronov, and G. E. Pikus, Zh. Eksp. Teor. Fiz. **69**, 1382 (1975). [Sov. Phys. JETP **42**, 705 (1975).]

[14] Y. Arakawa, and H. Sakaki, Appl. Phys. Lett. **40**, 939 (1982).

[15] A. T. Hanbicki, B. T. Jonker, G. Itskos, G. Kioseoglou, and A. Petrou, Appl. Phys. Lett. **80**, 1240 (2002).

[16] V. F. Motsnyi, J. D. Boeck, J. Das, W. V. Roy, G. Borghs, E. Goovaerts, and V, I, Safarov, Appl. Phys. Lett. **81**, 265 (2002).

[17] G. Salis, R. Wang, X. Jiang, R. M. Shelby, S. S. P. Parkin, S. R. Bank, and J. S. Harris, Appl. Phys. Lett. **87**, 262503 (2005).

[18] C. H. Li, G. Kioseoglou, O. M. J. van 't Erve, M. E. Ware, D. Gammon, R. M. Stroud, B. T. Jonker, R. Mallory, M. Yasar, and A. Petrou, Appl. Phys. Lett. **86**, 132503 (2005).

[19] X. Y. Dong, C. Adelmann, J. Q. Xie, C. J. Palmstrùm, X. Lou, J. Strand, P. A. Crowell, J.-P. Barnes, and A. K. Petford-Long, Appl. Phys. Lett. **86**, 102107 (2005).

[20] L. Lombez, P. Renucci, P. F. Braun, H. Carrère, X. Marie, T. Amand, B. Urbaszek, J. L. Gauffier, P. Gallo, T. Camps, A. Arnoult, C. Fontaine, C. Deranlot, R. Mattana, H. Jaffrès, J.-M. George, and P. H. Binh, Appl. Phys. Lett. **90**, 081111 (2007).

[21] B. S. Tao, P. Barate, J. Frougier, P. Renucci, B. Xu, A. Djeffal, H. Jaffrès, J.-M. George, X. Marie, S. Petit-Watelot, S. Mangin, X. F. Han, Z. G. Wang, and Y. Lu, Appl. Phys. Lett. **108**, 152404 (2016).

[22] K. Etou, S. Hiura, S. Park, K. Sakamoto, J. Takayama, A. Subagyo, K. Sueoka, and A. Murayama, Phys. Rev. Appl. **16**, 014034 (2021).

[23] K. Etou, S. Hiura, S. Park, J. Takayama, A. Subagyo, K. Sueoka, and A. Murayama, Phys. Rev. Appl. **19**, 024055 (2023).

[24] M. Paillard, X. Marie, P. Renucci, T. Amand, A. Jbeli, and J. M. Gérard, Phys. Rev. Lett. **86**, 1634 (2001).

[25] 舛本泰章，量子ドットの基礎と応用，裳華房 (2015).

[26] M. Sugawara, and M. Usami, Nat. Photonics **3**, 30 (2009).

[27] D. D. Awschalom, L. C. Bassett, A. S. Dzurak, E. L. Hu, and J. R. Petta, Science **339**, 1174 (2013).

[28] A. V. Khaetskii, and Y. V. Nazarov, Phys. Rev. B **61**, 12639 (2000).

[29] P. Borri, W. Langbein, S. Schneider, U. Woggon, R. L. Sellin, D. Ouyang, and D. Bimberg, Phys. Rev. Lett **87**, 157401 (2001).

[30] A. Tackeuchi, R. Ohtsubo, K. Yamaguchi, M. Murayama, T. Kitamura, T. Kuroda, and T. Takagahara, Appl. Phys. Lett. **84**, 3576 (2004).

[31] M. Paillard, X. Marie, P. Renucci, T. Amand, A. Jbeli, and J. M. Gerard, Phys. Rev. Lett. **86**, 1634 (2001).

[32] M. Kroutvar, Y. Ducommun, D. Heiss, M. Bichler, D. Schuh, G. Abstreiter, and J J. Finley, Nature **432**, 81 (2004).

Chapter 2. Research purpose

2.1 Previous works

2.1.1 Temperature dependence of optical spin properties of high-density quantum dots

To attain both high emission intensity and a substantial circular polarization degree at ambient temperature, comprehending the reasons for their decline at elevated temperatures is crucial. To address this, the temperature dependence of the optical spin properties of $In_{0.5}Ga_{0.5}As$ QDs with varying lateral QD densities (low-density or high-density QDs) has been investigated in this study [1]. Due to the smaller energy difference between $In_{0.5}Ga_{0.5}As$ and its excited state (ES) and the

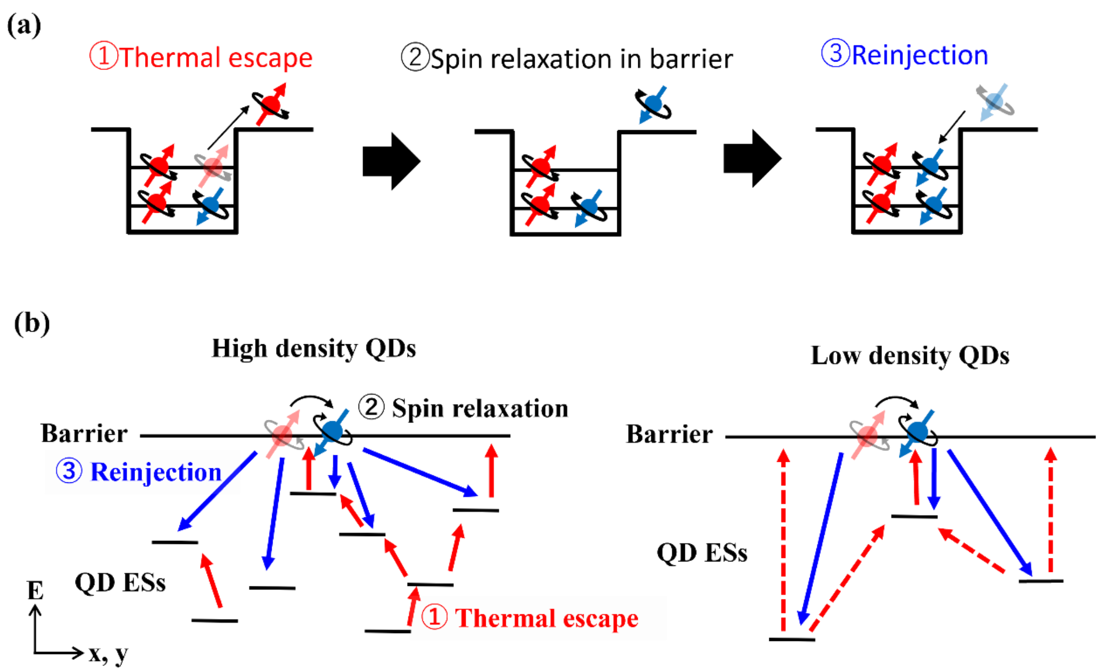

Figure 2-1. (a) Schematic model of electron-spin dynamics which result in low CPD at high temperature above 140 K. (b) Schematic illustration of the dynamics

surrounding GaAs barrier compared to InAs, it proves conducive for probing the impacts of thermal escape.

In our investigation, it was observed that high-density QDs exhibit diminished emission intensity and circular polarization degree compared to low-density QDs at temperatures exceeding 140 K. Figure 2-1 schematically illustrates the model of electron-spin dynamics at elevated temperatures. For both low- and high-density QDs, a sequence of events unfolds, as depicted in Figure 2-1(a). Initially, electron spins thermally escape from the QD to the surrounding barrier. Subsequent to thermal escape, electron spins undergo rapid relaxation within the barrier via the DP spin relaxation process [2, 3, 4, 5], given the semiconductor bulk nature of the barrier layer. Ultimately, spin-flipped electron spins are reintroduced into the QD states, resulting in a reduction of the circular polarization degree. Additionally, in the case of high-density QDs, the strong coupling of electron wavefunctions among QDs, due to their close proximity, induces interdot spin transfer and accelerates thermal escape, leading to a lower circular polarization degree. These findings underscore the significance of suppressing electron spin relaxation in the surrounding barrier layer and enhancing the spin polarization degree of reintroduced electron spins for achieving a high circular polarization degree at elevated temperatures. Thus, the suppression of DP spin relaxation at the barrier, facilitated by p-doping, enhances the circular polarization degree of QD emission [6].

2.1.2 Spin filtering effect in dilute nitride GaAs

As detailed in the preceding chapter, one viable approach to achieving a high CPD at elevated temperatures involves enhancing the spin polarization degree of electrons reintroduced into QDs. To pursue this objective, we explored the utilization of dilute nitride GaNAs, known for amplifying conduction band electron spin polarization at ambient temperature through spin-dependent recombination, as elucidated below. A previous study comparing nitrogen-free InGaAs QWs with $InGa_{0.994}N_{0.006}As$ QW reported higher CPD and a twentyfold increase in electron spin relaxation time at ambient temperature [7]. This observation extends beyond QWs, as the spin relaxation time in the bulk $InGaAs_{0.988}N_{0.012}$ layer increases with temperature, rendering it suitable for high-temperature operation.

Spin-polarized defect levels play a pivotal role in spin-dependent recombination, contributing to the CPD amplification. In dilute GaNAs, nitrogen-induced defect-related localized states (LSs) are energetically deep within the band gap. These LSs are intricately coupled to the conduction band, enabling them to capture conduction band electrons. Upon injection of spin-polarized electrons into GaNAs, the LSs themselves become spin-polarized. The mechanism of spin polarization of LSs is illustrated in Figure 2-2 (1). In the initial state A, LSs are unpolarized. Upon the arrival of spin-polarized electrons, as depicted in B, LSs capture electrons in accordance with the Pauli principle. As illustrated in C, within LSs housing two electrons, one electron and a hole recombine, restoring the LSs to a state with only one electron. Following several cycles of B and C, the LSs become spin-polarized, as shown in D. Figure 2-2 (2) is the detailed illustration of the LSs spin-polarization with more electrons and holes to help understanding.

2.2 Purpose of this work

In pursuit of attaining both high emission intensity and a significant CPD at ambient temperature, our emphasis has been on exploring the spin filtering effect of dilute nitride GaNAs. The discussion on electron spin dynamics, detailed in the various studies below, is undertaken with the objective of identifying the optimal device structure capable of effectively converting electron spin into circularly polarized light.

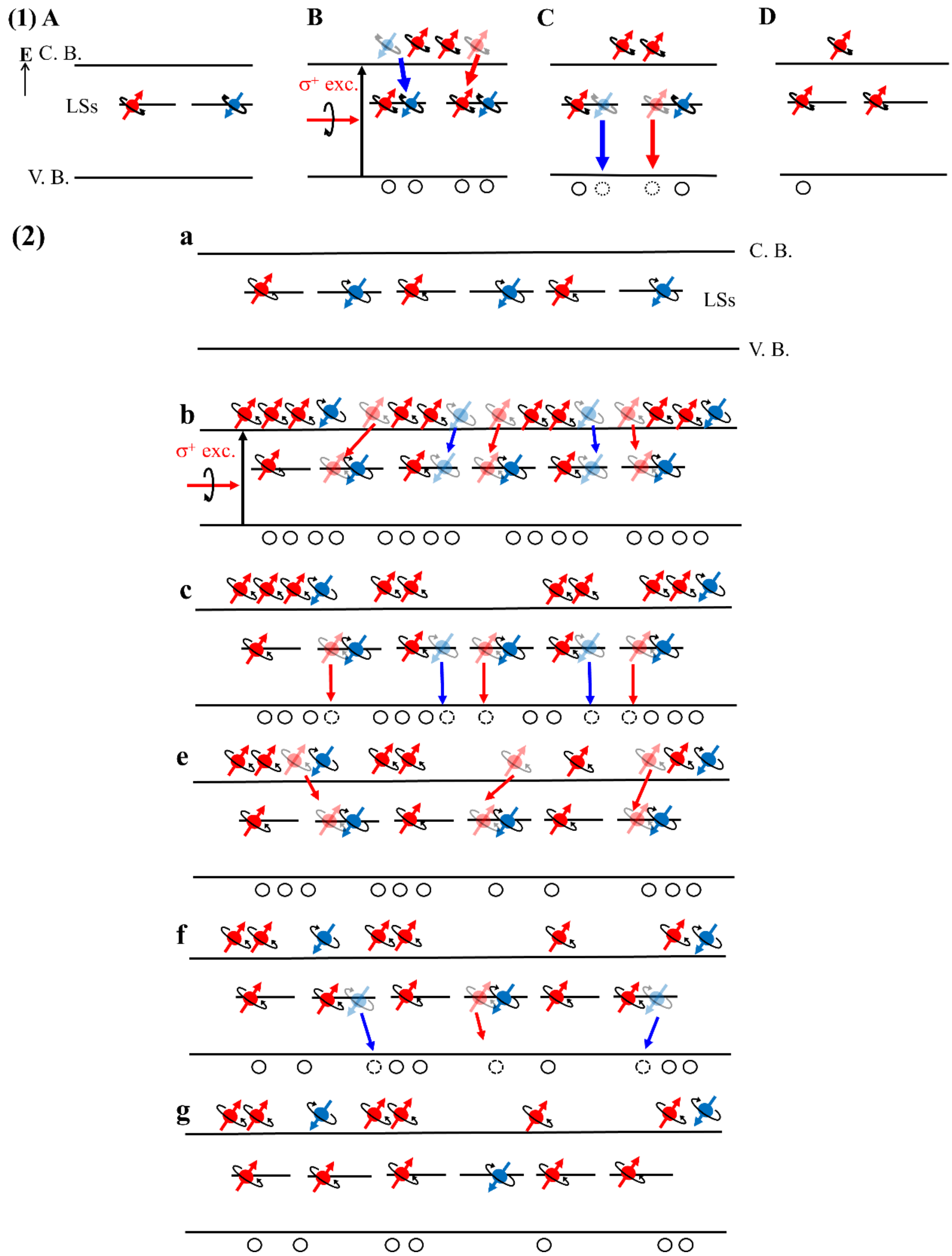

Figure 2-2. (1) Schematic diagram of the mechanism of spin polarization of LSs. Black open circles represent holes. (2) Detailed illustration of the spin-polarization phenomena of LSs with more carriers.

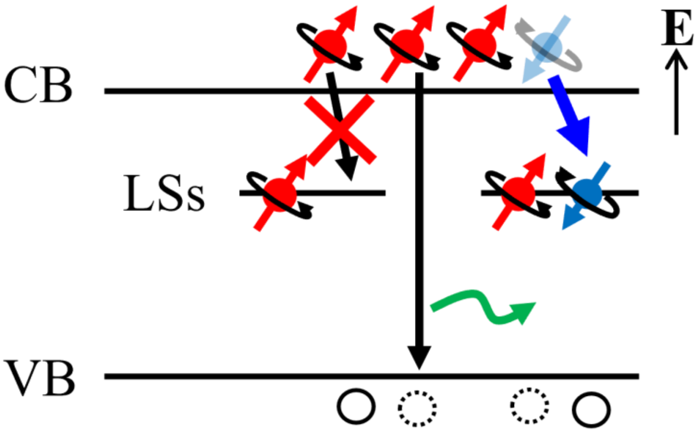

Figure 2-3. Schematic illustration of the spin dependent recombination.

References

[1] S. Sato, S. Hiura, J. Takayama, and A. Murayama, J. Appl. Phys. **127**, 043904 (2020).

[2] M. Paillard, X. Marie, P. Renucci, T. Amand, A. Jbeli, and J. M. Gérard, Phys. Rev. Lett. **86**, 1634 (2001).

[3] A. V. Khaetskii, and Y. V. Nazarov, Phys. Rev. B **61**, 12639 (2000).

[4] P. Borri, W. Langbein, S. Schneider, U. Woggon, R. L. Sellin, D. Ouyang, and D. Bimberg, Phys. Rev. Lett **87**, 157401 (2001).

[5] A. Tackeuchi, R. Ohtsubo, K. Yamaguchi, M. Murayama, T. Kitamura, T. Kuroda, and T. Takagahara, Appl. Phys. Lett. **84**, 3576 (2004).

[6] S. Sato, S. Hiura, J. Takayama, and A. Murayama, Appl. Phys. Lett. **116**, 182401 (2020).

[7] D. Lagarde, L. Lombez, X. Marie, A. Balocchi, T. Amand, V. K. Kalevich, A. Shirayaev, E. Ivchenko and A. Egorov, phys. stat. sol. (a) **204**, 208 (2007).

Chapter 3. Experimental Procedures

3.1 Sample growth by Molecular beam epitaxy (MBE) method

III-V compound semiconductor QDs were fabricated using MBE equipped with a radiofrequency (RF) plasma source for nitrogen. MBE, a crystal growth technique, involves the epitaxial growth of a single crystal film by directing source materials, evaporated through heating or other methods, onto a substrate within an ultra-high vacuum growth chamber. In RF plasma-assisted MBE, nitrogen is introduced as nitrogen plasma. Figure 3-1 (a) provides a schematic depiction of the MBE growth chamber [1]. The ultra-high vacuum conditions within the growth chamber allow for an exceptionally slow growth rate, ensuring high crystal quality. This setup facilitates precise control of film thickness at the scale of one atomic layer and the creation of well-defined step hetero-interfaces. Within the MBE process, each raw material—such as gallium, arsenic, and indium—is housed in a Knudsen cell (K-cell). Each K-cell is equipped with a shutter that can be mechanically opened and closed, along with a heater for temperature regulation. The shutters control the timing

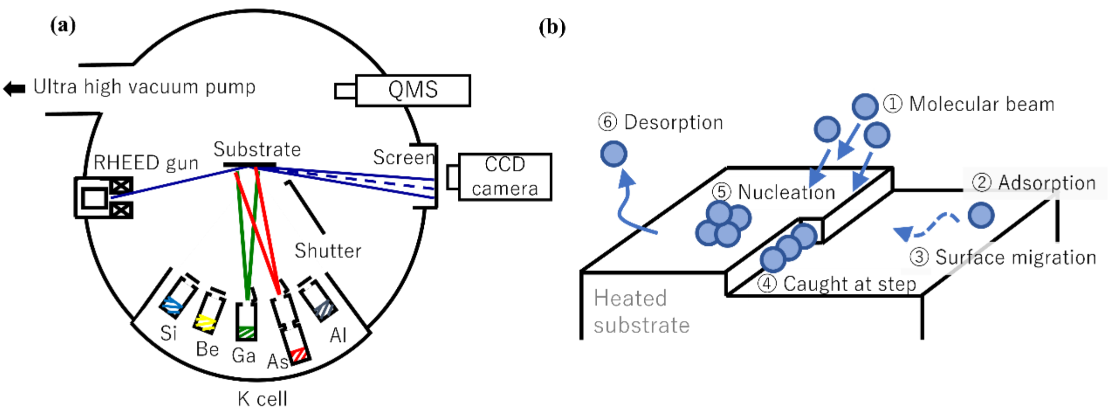

Figure 3-1. (a) Schematic image of MBE growth chamber (made while referencing [1]) and (b) Schematic diagram of Kossel mechanism of MBE epitaxial growth (made while referencing [2]).

of material supply, while the temperature controls the supply rate, ensuring meticulous control over the growth process.

3.2 Sample structures

All samples elucidated in this dissertation feature a 300-nm-thick GaAs buffer layer on the GaAs (100) substrate. The fabrication of samples involving varying tunnel-barrier thicknesses (discussed in Chapter 5), samples with different GaNAs quantum well (QW) thicknesses (expounded in Chapter 6), and samples with different GaNAs QW positions (detailed in Chapter 7) followed a consistent set of growth processes.

3.2.1 Growth procedure of samples with different tunnel-barrier thickness

Following the growth of a GaAs buffer layer exceeding 300 nm on the GaAs (100) substrate, a 20-nm-thick dilute nitride GaNAs layer was deposited. The RF power during the GaNAs growth was maintained at 70 W. Subsequently, the GaAs tunnel barrier and subsequent InAs quantum dots (QDs) were grown. Two samples were prepared with different tunnel barrier thicknesses: d = 3 and 10 nm. Finally, an additional 100-nm-thick GaAs capping barrier and the InAs QD layer, intended for structural observations, were subsequently grown.

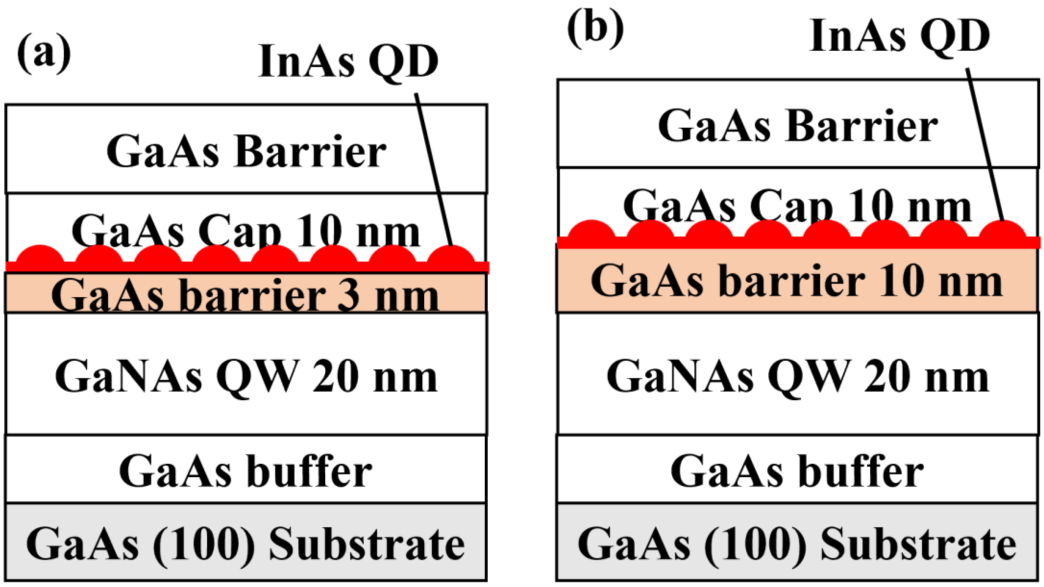

Figure 3-2. Schematic images of InAs QD - GaNAs QW tunnel-coupled structure with different GaNAs QW thicknesses with different GaAs tunnel-barrier thicknesses.

3.2.2 Growth procedure of samples with different GaNAs QW thickness

Following the growth of a 300-nm-thick GaAs buffer layer on the GaAs (100) substrate, a dilute nitride GaNAs layer was deposited. The nominal nitrogen concentration was set at 1%, and three samples were created with varying GaNAs QW thicknesses: $d = 5$, 10, and 20 nm. Subsequently, a 3-nm-thick GaAs tunnel barrier and the ensuing InAs quantum dots (QDs) were grown. To conclude, an additional 100-nm-thick GaAs capping barrier and the InAs QD layer, intended for structural observations, were subsequently grown.

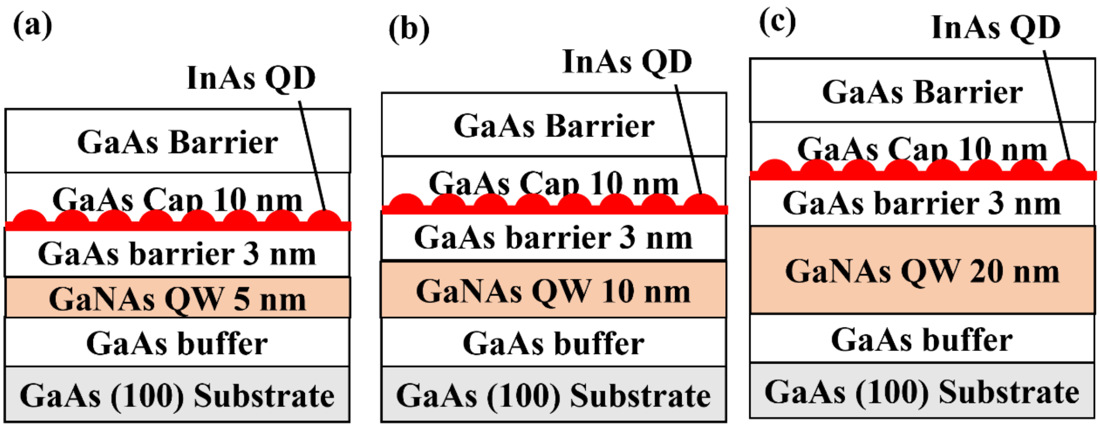

Figure 3-3. Schematic images of InAs QD - GaNAs QW tunnel-coupled structure with different GaNAs QW thicknesses.

3.2.3 Sample structures of samples with different GaNAs QW position

We fabricated three samples with distinct configurations, positioning the GaNAs QW in different locations relative to the InAs QD. Specifically, sample a had the GaNAs QW beneath the InAs QD, sample b had it above the InAs QD, and sample c featured GaNAs QWs on both the upper and lower sides of the InAs QD. The GaNAs QW thickness for samples a and b was 10 nm, while sample c incorporated a 5-nm-thick GaNAs QW on both sides, resulting in a total GaNAs QW thickness of 10 nm for all three samples. A 10-nm-thick GaAs layer capped the InAs QDs. For samples a and c, a 3-nm-thick GaAs tunnel barrier was introduced between the InAs QD layer and the lower side GaNAs layer. Additionally, all three samples included an extra GaAs capping barrier and an InAs QD layer to facilitate structural observations.

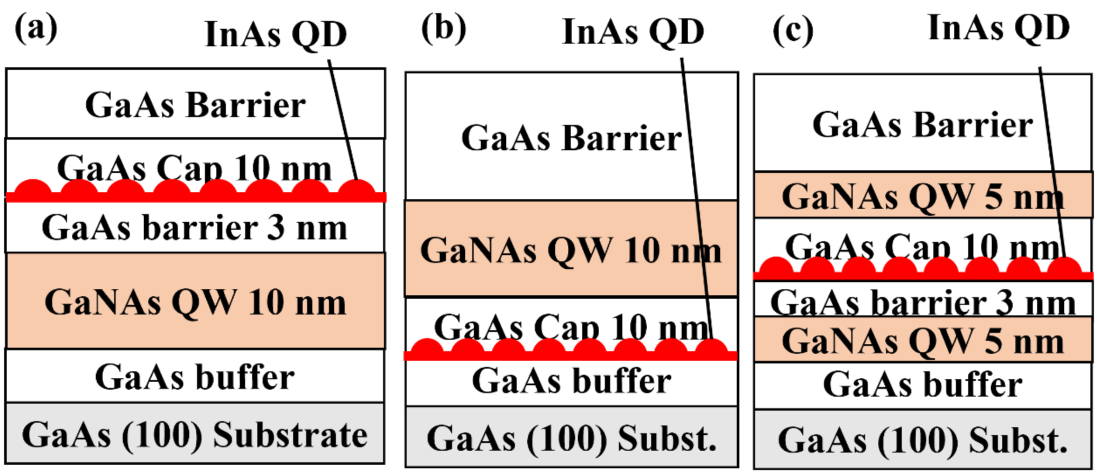

Figure 3-4. Schematic images of InAs QD - GaNAs QW tunnel-coupled structure, whose QW layers exist (a) lower side, (b) upper side and (c) both sides of the QD layer.

3.3 Circularly polarized photoluminescence measurement

In this investigation, the optical spin properties of the fabricated samples were assessed through time-resolved circularly polarized photoluminescence (PL) measurements. Figure 3-5 illustrates the diagram of the measurement system, while Figure 3-6 provides a schematic representation of the measurement principle. The

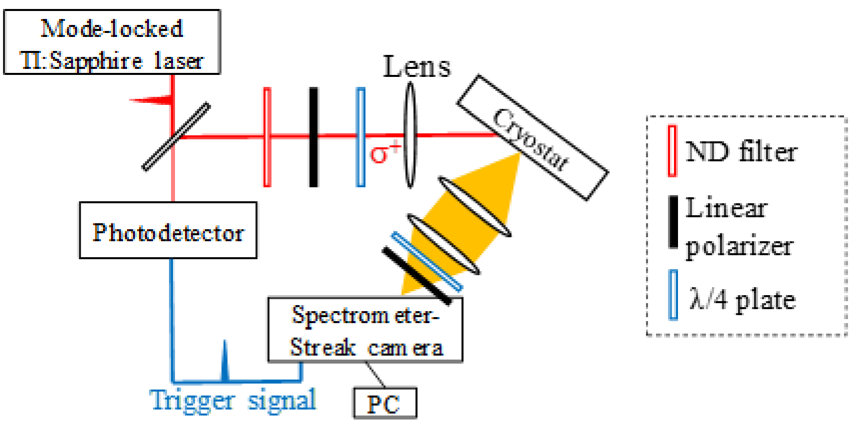

Figure 3-5. Measurement system of circularly polarized time-resolved PL measurement.

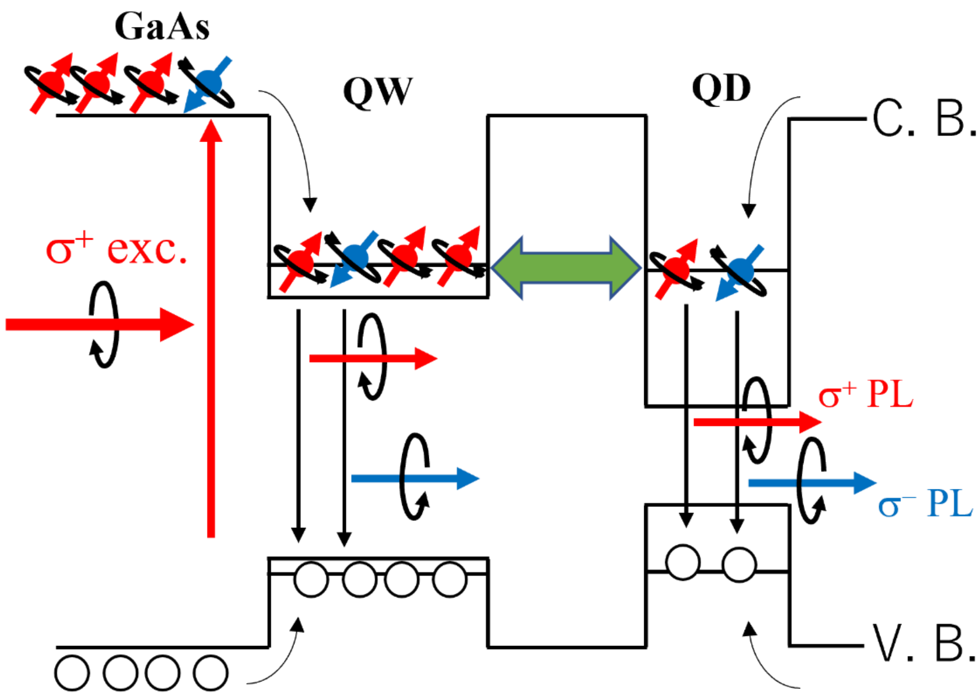

Figure 3-6. Schematic diagram of the measurement principle.

experimental setup involved an excitation laser with a wavelength of 800 nm, emitted by a mode-locked Ti:Sapphire laser. This laser was converted into s+ circularly polarized light using a linear polarizer and a quarter-wave plate (λ/4 plate). The s+ polarized laser was then directed onto the sample within a cryostat, where spin-polarized carriers were generated in the GaAs barrier layer. The initial spin polarization degree was set at 50%, aligning with the optical selection rule [3]. Subsequently, the generated spin-polarized carriers were injected into QDs and QWs through energy relaxation, leading to the radiative recombination of electron-hole pairs. If the electron spin is conserved until the emission, s+ circularly polarized photoluminescence (PL) is detected. Conversely, if the electron spin undergoes flipping, s- circularly polarized PL is observed. A λ/4 plate and a linear polarizer were strategically employed to construct a filter, allowing the selective measurement of PL in either the s+ or s- circularly polarized state from the sample. This setup facilitated the separate measurement of PL in each circularly polarized state.

3.4 Rate equation

To simulate circularly polarized PL time profiles, we used a rate-equation model including tunnel spin transfer and relaxation processes in the GaNAs QW and InAs QD tunnel-coupled system [4]. The rate-equation model is shown in Figure 3-7(a). In this model, we considered the spin-selective relaxation from the QD GS to the GaNAs LSs. In addition, the GS PL was defined as the sum of the PL derived from the carriers injected from the GaAs barriers and GaNAs QW because the GaAs barrier was photoexcited in this study. The first PL component includes the number of carriers in the GaAs barrier N_b, a spin conservation factor during the injection process a_b. Parameters τ_r, τ_s and τ_{inj}^{b} denote the time constants for radiative recombination, spin relaxation, and spin injection from the barrier to QDs, respectively. The rate equation can be written by the following Equations 3-1 to 3-3. Herein, $N_{QD\sigma+}(N_{QD\sigma-})$ implies the population of the QD GS with majority (minority) spin.

$$\frac{dN_b}{dt} = -\frac{a_b \times N_b}{\tau_{inj}^{b}} - \frac{(1-a_b)\times N_b}{\tau_{inj}^{b}} \qquad (3-1)$$

$$\frac{dN_{QD\sigma+}}{dt} = \frac{a_b \times N_b}{\tau_{inj}^{b}} + \frac{N_{QD\sigma-}}{\tau_s} - \frac{N_{QD\sigma+}}{\tau_s} - \frac{N_{QD\sigma+}}{\tau_r} \qquad (3-2)$$

$$\frac{dN_{QD\sigma+}}{dt} = \frac{(1-a_b)\times N_b}{\tau_{inj}^{b}} + \frac{N_{QD\sigma+}}{\tau_s} - \frac{N_{QD\sigma-}}{\tau_s} - \frac{N_{QD\sigma-}}{\tau_r} \qquad (3-3)$$

For the second PL component derived from the carriers injected from the GaNAs QW, the number of carriers in the GaNAs QW and a spin conservation factor during the injection process are expressed as N_{QW} and a_{QW}, respectively. Herein, a_{QW} depends on the spin filtering effect of GaNAs. Parameter τ_{inj}^{QW} denotes the time constant for spin injection from the QW to QD. In particular, τ_{inj}^{QW} is the effective time constant and includes the reverse spin transfer from the QD to QW via thermal redistribution. Only for the QD-emission components, the time constant for the capture of majority (minority) spins by the LSs is defined as $\tau_{c+}(\tau_{c-})$, whereas this LS contribution before the spin injection into the QDs is included in the a_{QW} term, as described above. Because the radiative recombination and spin relaxation occur inside the QDs, τ_r and τ_s were assumed to be the same for electron spins injected from the GaAs barrier and GaNAs QW. The rate equation can be written by following Equations 3-4 to 3-6.

$$\frac{dN_{QW}}{dt} = -\frac{a_{QW} \times N_{QW}}{\tau_{inj}^{QW}} - \frac{\left(1 - a_{QW}\right) \times N_{QW}}{\tau_{inj}^{QW}} \qquad (3-4)$$

$$\frac{dN_{QD\sigma+}}{dt} = \frac{a_{QW} \times N_{QW}}{\tau_{inj}^{QW}} + \frac{N_{QD\sigma-}}{\tau_s} - \frac{N_{QD\sigma+}}{\tau_s} - \frac{N_{QD\sigma+}}{\tau_r} - \frac{N_{QD\sigma+}}{\tau_{c+}} \qquad (3-5)$$

$$\frac{dN_{QD\sigma+}}{dt} = \frac{\left(1 - a_{QW}\right) \times N_{QW}}{\tau_{inj}^{QW}} + \frac{N_{QD\sigma+}}{\tau_s} - \frac{N_{QD\sigma-}}{\tau_s} - \frac{N_{QD\sigma-}}{\tau_r} - \frac{N_{QD\sigma-}}{\tau_{c-}} \qquad (3-6)$$

Figures 3-7(b, c, d) present the simulation results of the proposed rate equation, showcasing the time-dependent characteristic CPD amplification with well-reproduced outcomes using appropriate parameters. Figure 3-7(b) presents the simulation results with various N_b at a fixed N_{QW} = 60 and a_{QW} = 0.8, where the larger contribution of the spin injection from the GaNAs QW to that from the GaAs barrier causes a stronger CPD amplification. The effect of on the time-dependent CPD is evident from the results plotted in Figure 3-7(c), where parameters τ_{c-} = 10 ps and N_{QW}/N_b = 1.5 are fixed. When the occupancy of the LSs by majority spins is high, τ_{c+} increases owing to Pauli blocking. In this case, majority spins are likely to remain in the QDs relative to the transfer of minority spins from the QDs to LSs, resulting in a stronger CPD amplification. Moreover, Figure 3-7(c) indicates that the increase in τ_{c+} can suppress the CPD decay in the second-half time range. In contrast, the decrease in τ_{inj}^{QW} results in rapid CPD amplification (Figure 3-7(d)).

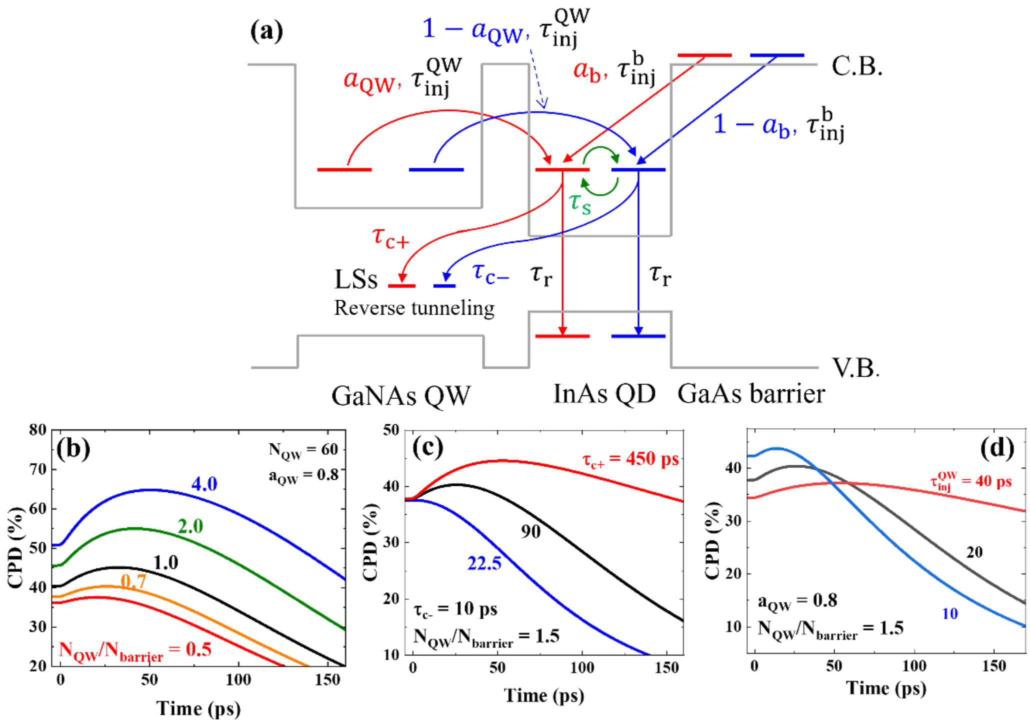

Figure 3-7. (a) Rate equation model including tunnel spin transfer and relaxation processes in tunnel-coupled system of GaNAs QW and InAs QD. Simulation results of rate equations with various (b) N_b (c) τ_{c+} and (d) τ_{inj}^{QW}.

References

[1] 権田俊一，アドバンストエレクトロニクスＩ-10 分子線エピタキシー，培風館 (1994).

[2] A. Kaneko, and Y. Furukawa, Seimitsu Kogaku Kaishi / Journal of the Japan Society for Precision Engineering, **66**, 735 (2000).

[3] F. Meier and B. Zakharchenya, Optical Orientation, (Elsevier, North-Holland, Amsterdam, 1984).

[4] Shino Sato, Satoshi Hiura, Junichi Takayama, and Akihiro Murayama, Applied Physics Letters **123**, 232405 (2023).

Chapter 4. High electron spin polarization degree at ambient-temperature with InGaAs QD–GaNAs QW tunnel-coupled structure

4.1 Background

This chapter delves into the exploration of high electron spin polarization in the InGaAs quantum dot (QD) — GaNAs quantum well (QW) tunnel-coupled structure, as discussed in the work authored by Yuqing Huang et al. [1]. My involvement in this study primarily centered on PL measurements.

In conventional semiconductors, the steady-state electron spin polarization, $P_e = \frac{n_\uparrow - n_\downarrow}{n_\uparrow + n_\downarrow}$, is represented by Equation (4-1) [2].

$$P_e = \frac{P_0}{1 + \tau/\tau_s} < P_0\,, \qquad (4-1)$$

τ_s is the electron spin-relaxation time, τ is the electron lifetime, and P_0 is the initial spin-polarization degree. This equation demonstrates that the electron spin-polarization, P_e, is limited by initial the spin-polarization, P_0. To overcome this strict limitation, spin filtering effect via a spin-dependent recombination process in GaNAs have attracted attention. Under the spin filtering effect, electron lifetime of majority- and minority-spin are no longer equal; accordingly, Equation (4-1) is modified as follows:

$$P_e = \frac{(1+P_0)\,\tau_\uparrow/\tau_\downarrow - (1-P_0)}{(1+P_0)\,\tau_\uparrow/\tau_\downarrow + (1-P_0) + 2\tau_\uparrow/\tau_s}, \qquad (4-2)$$

$\tau_\uparrow(\tau_\downarrow)$ denotes the lifetime of the spin-up (spin-down) conduction band electrons. Theoretically, $|P_e|$ can exceed $|P_0|$ via the spin filtering effect. However, when the spin filtering layer (GaNAs) is used as the optically active layer, defects and potential fluctuations in the GaNAs layer degrade the electron spin polarization. Therefore, the author proposed a concept termed remote spin filtering. They prepared the sample with a GaNAs QW as a spin filtering layer and an InAs QD layer as an optically active layer. They achieved over 90% electron spin polarization at ambient temperature, demonstrating the efficacy of the two-step remote spin filtering.

4.2 Two-step remote filtering

To achieve heightened electron-spin polarization through remote spin-filtering at ambient temperature, the authors introduced the concept of two-step remote spin filtering. The first step involves standard spin filtering, where conduction-band electron spins undergo filtration in GaNAs, as detailed in Section 2.1.2 [3]. Additionally, when the electron ground state (referred to as e0 in this paper) of the

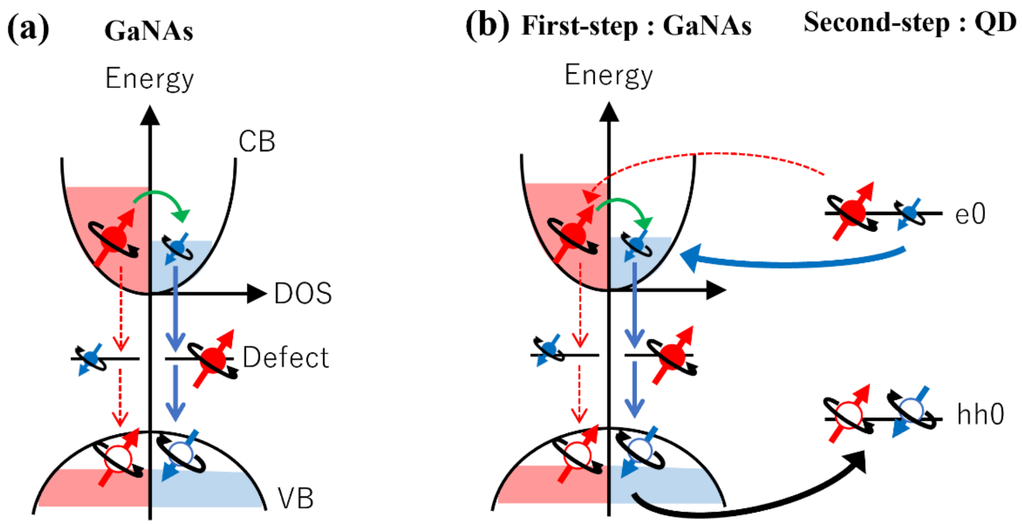

Figure 4-1. (Made while referencing Fig.2a and 2b of [1]) Principle of the defect-enabled remote spin filtering. A simplified picture of the working principle of single-step, defect-enabled spin filtering in GaNAs (a) and the two-step remote spin filtering in a coupled QD/GaNAs nanostructure (b). The size of electron spins illustrates the number of them.

QDs lies between the occupation levels of majority and minority spins in GaNAs, as illustrated in Figure 4-1, a two-step spin filtering mechanism can be realized. The second step involves the injection of majority spins into QDs and simultaneous removal of minority spins from QDs. This is facilitated by the distinctly aligned energy states shown in Figure 4-1(b), where majority spins exhibit a tendency to occupy QD ground states, while minority spins preferentially reside in the GaNAs level [4]. This innovative two-step remote spin filtering strategy contributes to achieving enhanced electron-spin polarization under ambient conditions.

4.3 Sample structure

A schematic of the studied samples is presented in Figure 4-2. The samples feature an InAs QDs layer tunnel-coupled with a GaNAs spin-filtering layer separated by a thin GaAs tunneling barrier layer. A reference QD sample (ref-QD) and reference GaNAs sample (ref-GaNAs) were also studied for a comparative analysis. Samples with different N concentrations (1 to 2.6%) in GaNAs and different GaAs tunneling barrier thicknesses (3 to 15 nm) were prepared to investigate the effects of two-step remote spin filtering. The samples with a N concentration of 1.5% and GaAs tunnel barrier thickness of 3 nm exhibited the highest QD electron spin polarization, $|P_e^{QD}|$, of 90%.

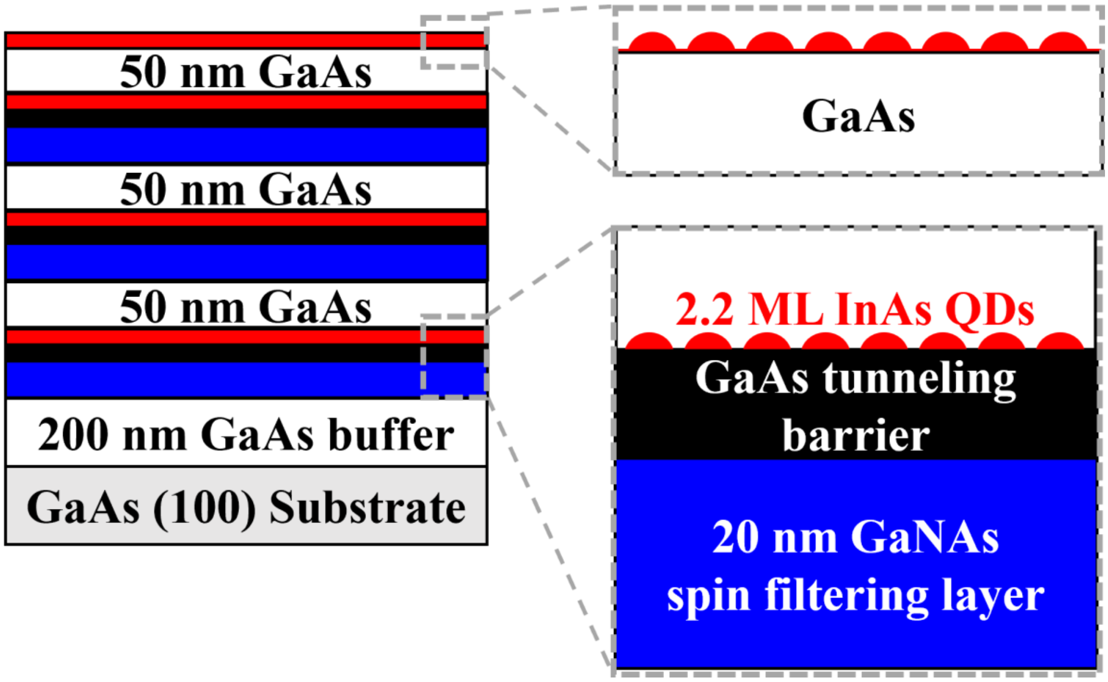

Figure 4-2. (Made while referencing Figure S1 of [1]) Schematic illustration of the studied QD / GaNAs nanostructures.

4.4 Results and discussion

4.4.1 PL measurements

The polarization-resolved PL spectra are illustrated in Figures 3 (d, e, f) of [1]. The QD/GaNAs sample and reference GaNAs samples were excited with continuous-wave σ^+-polarized laser above the GaNAs bandgap. σ^+/σ^+ (σ^+/σ^-) (Figure 3 of [1]) implies σ^+-excitation/σ^+-detection (σ^+-excitation/σ^--detection). The reference QD sample was excited above the GaAs bandgap. Considering the spin loss from carrier generation to energy relaxation, the initial spin polarization of electron in the GaNAs conduction band, P_0^{GaNAs}, can be estimated to be less than 10% [5]. First, comparing the PL energies, the PL energies of the QD/GaNAs samples correspond to those of the reference QD (Figure 3(e) of [1]) and reference GaNAs sample (Figure 3(f) of [1]), respectively. The QDs in QD/GaNAs exhibit a PL polarization, P_{PL}, of 90% at ambient temperature, a significant increase compared to the reference QD with a P_{PL} of 2%.

4.4.2 Time-resolved PL measurements

Time-resolved PL measurements were performed to confirm that the observed high P_{PL} originated from the spin filtering effects. Figure 4 (a) of [1] presents the decay curves of I_{PL}^{QD} and P_{PL}^{QD} from the ref-QD and QD/GaNAs structure with a GaAs tunneling barrier thickness of 3 nm. In the case of the ref-QD, σ^+ PL and σ^- PL converge to identical values after the electron spins are completely relaxed. In contrast, those of QD/GaNAs do not converge to identical values, and the initial decay of the σ^+ PL is slower than the σ^- PL. This discrepancy serves as compelling evidence that the remote spin filtering is the underlying cause of the remarkably high $|P_e^{QD}|$ of 90% at ambient temperature.

Furthermore, the authors investigated the effects of barrier thickness and enegy-level alignment. Especially, in experiments with various N concentrations, the maximum $|P_e^{QD}|$ of 90% was attributed to the maximum overlap achieved between the GaNAs and QD. This emphasizes the significance of barrier thickness and energy-level alighnment in influencing and maximizing electron spin polarization.

4.5 Conclusion

In conclusion, a significant milestone was reached in achieving a remarkable electron spin polarization of 90% through the innovative approach of coupling InAs QDs with GaNAs using a two-step filtering effect. This outcome serves as clear and compelling evidence that remote spin filtering is an effective strategy for enhancing high electron spin polarization and, consequently, achieving a notable circularly polarization degree at ambient temperature.

References

[1] Y. Huang, V. Polojärvi, S. Hiura, P. Höjer, A. Aho, R. Isoaho, T. Hakkarainen, M. Guina, S. Sato, J. Takayama, A. Murayama, I. A. Buyanova and W. M. Chen, Nat. Photonics **9**, 259 (2015).

[2] F. Meier and B. Zakharchenya, Optical Orientation, (Elsevier, North-Holland, Amsterdam, 1984).

[3] D. Lagarde, L. Lombez, X. Marie, A. Balocchi, T. Amand, V. K. Kalevich, A. Shirayaev, E. Ivchenko and A. Egorov, phys. stat. sol. (a) **204**, 208 (2007).

[4] C. E. Pryor and M. E. Flatte, Phys. Rev. Lett. **96,** 026804 (2006).

[5] Y. Puttisong, I. A. Buyanova, A. J. Ptak, C. W. Tu, L. Geelhaar, H. Riechert. and W. M. Chen, adv. Mater. **25**, 738 (2013).

Chapter 5. Tunnel-barrier thickness dependence of optical spin properties of InAs QDs

5.1 Background

Building upon earlier research [1] detailed in the preceding chapter, the GaNAs QW–InAs QD tunnel-coupled nanostructure proves effective in achieving heightened electron spin polarization and corresponding CPD at ambient temperature. To comprehensively understand the impact of various parameters and optimize the sample structure, our initial focus is on studying the dependence of optical spin properties of InAs QDs on tunnel-barrier thickness. While some investigations on tunnel barrier thickness effects have been conducted in prior studies [1], this research aims to deepen our understanding by examining samples grown in-house with our specialized equipment. This approach is geared towards accumulating knowledge for the fabrication of diverse structures incorporating GaNAs and QDs in future endeavors.

5.2 Experimental procedures

5.2.1 Sample structures

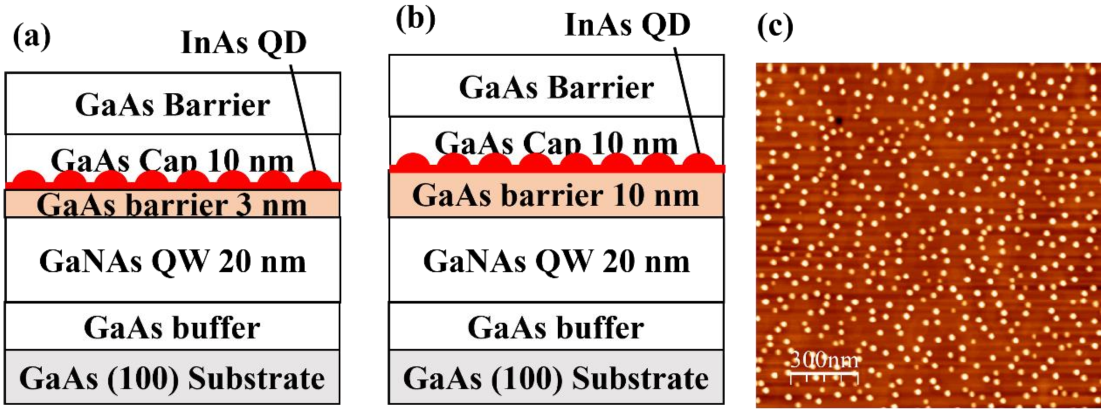

Figure 5-1. (a,b) Schematic images of InAs QD–GaNAs QW tunnel-coupled structure with different GaAs tunnel-barrier thicknesses. (c) The atomic force microscopy (AFM) image of the InAs QD grown on the top of the sample for AFM analysis (not shown in Figures 5a and 5b).

Schematic images of InAs QD–GaNAs QW tunnel-coupled structure are presented in Figures 5-1(a, b). Two samples were grown with identical conditions except for the GaAs tunnel barrier thickness $d = 3$ or 10 nm. The detailed growth conditions are described in Chapter 3.1.1. Figure 5-1(c) illustrates the atomic force microscopy (AFM) image of the InAs QD grown on top of the sample. The areal QD density is estimated as 2.5×10^{10} cm^{-2}. It is worth noting that a strict energy alignment was not employed, potentially impacting the occurrence of the two-step spin filtering process [1, 2].

5.2.2 Circularly polarized time-resolved PL measurement

The circularly polarized time-resolved photoluminescence (PL) was conducted at ambient temperature, with the excitation energy set to 1.46 eV to induce spin-polarized carriers in the GaAs barriers. It is crucial to highlight a significant departure from the previous study [1], where carrier generation occurred in the GaNAs quantum well (QW).

5.3 Results and discussion

5.3.1 Circularly-polarized PL spectra

Figure 5-2 (a) presents the circularly polarized PL spectra recorded at ambient temperature. The red solid lines indicate σ^{+}-PL, which denotes spin-conserved emission, and the blue solid lines indicate σ—PL, which implies the spin-flipped emission. The green solid lines represent the corresponding CPD spectra determined by Equation (5).

$$CPD\ (\%) = \frac{I_{\sigma+} - I_{\sigma-}}{I_{\sigma+} + I_{\sigma-}} \times 100, \tag{5}$$

where, $I_{\sigma\pm}$ denotes the intensity of $\sigma^{\pm}$-PL. The lower-energy emissions originate from the QD emissive states, and the higher-energy emissions originate from the GaNAs QW.

The *d* = 10-nm sample achieves a maximum CPD of approximately 15%. In contrast, the *d* = 3-nm samples exhibited a CPD exceeding 30% at ambient temperature. Figure 5-2 (b) presents the average CPD of QD emission as a function of the excitation power, and the *d* = 3-nm sample showcases a substantial enhancement in CPD across all excitation power levels.

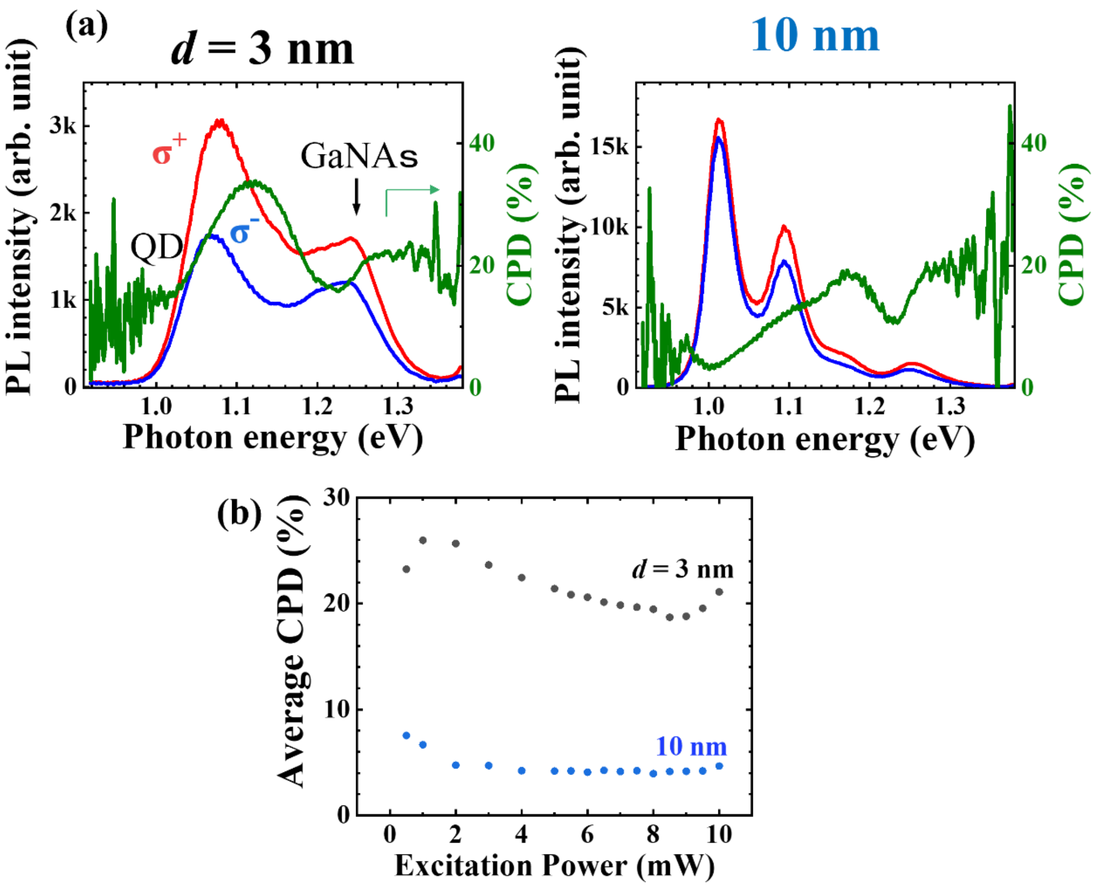

Figure 5-2. (a) Circularly polarized PL spectra and corresponding CPD of InAs QD – GaNAs tunnel-coupled samples with *d* = 3 and 10 nm, measured at room temperature. (b) Average CPD of QD emission as a function of excitation power.

5.3.2 Discussion from PL spectra and PL decay

Initially, we delved into the intricacies surrounding the enhanced CPD by exploring the spin-independent PL spectra and PL decay time. Figure 5-3 unveils the normalized PL spectra emanating from samples with tunnel barrier thicknesses of *d* = 3 and 10 nm. Upon scrutinizing the ratio of PL intensity originating from QDs to that from GaNAs, a conspicuous disparity surfaces in the *d* = 3 nm sample. This discrepancy is rooted in the prevalence of dominant electron spin tunneling from QD to GaNAs, propelled by the robust coupling of electron wavefunctions, ushering in a

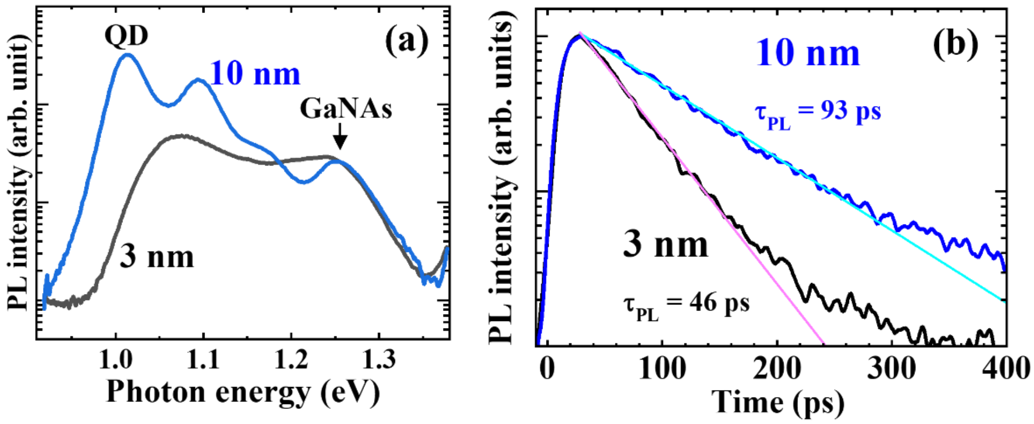

Figure 5-3. Ambient-temperature PL spectra normalized by PL intensity of GaNAs (a) and QD-PL time profiles (b) of InAs QD – GaNAs QW tunnel-coupled samples with d = 3 nm (black solid line) and d = 10 nm (blue solid line).

larger influx of electrons from QDs to GaNAs. Turning our attention to Figure 5-3(b), a compelling narrative unfolds through time-resolved PL from QDs in both samples. The PL decay time for the d = 3 nm sample clocks in at 46 ps, a stark contrast to the 93 ps observed in its d = 10 nm counterpart. This expedited PL decay underscores a more potent coupling of electron wavefunctions between GaNAs and QDs, indicative of a more efficacious electron spin tunneling trajectory from QDs into GaNAs for the d = 3 nm sample.

5.3.3 Discussion from transient spin polarization properties

Figures 5-4 presents the ambient temperature time-resolved circularly PL and the corresponding CPD of QDs. The initial CPD for the d = 10 nm sample registers at approximately 20%. In contrast, the d = 3 nm sample exhibits a notably higher initial CPD, reaching about 35%. Moreover, the d = 3 nm sample manifests a temporal amplification of CPD, peaking at 50% around 90 ps. This pronounced initial CPD and the subsequent amplification observed in the d = 3 nm sample can be ascribed to the robust influence of the spin filtering effect of GaNAs [1, 3, 4]. Two conceivable mechanisms are posited as contributors to the heightened CPD in the $d = 3$ nm sample.

The first mechanism involves the tunnel injection of highly-polarized electron spins from the GaNAs QW to the InAs QD, as illustrated in Figure 5-5 (a). As discussed in Chapter 2.1.2, GaNAs has the capability to amplify the spin polarization of conduction band electrons due to the spin filtering effect [1, 3, 4]. In the case of the $d = 3$ nm sample, where GaNAs QW and QDs are strongly coupled, this effect becomes more pronounced, resulting in the amplified initial CPD.

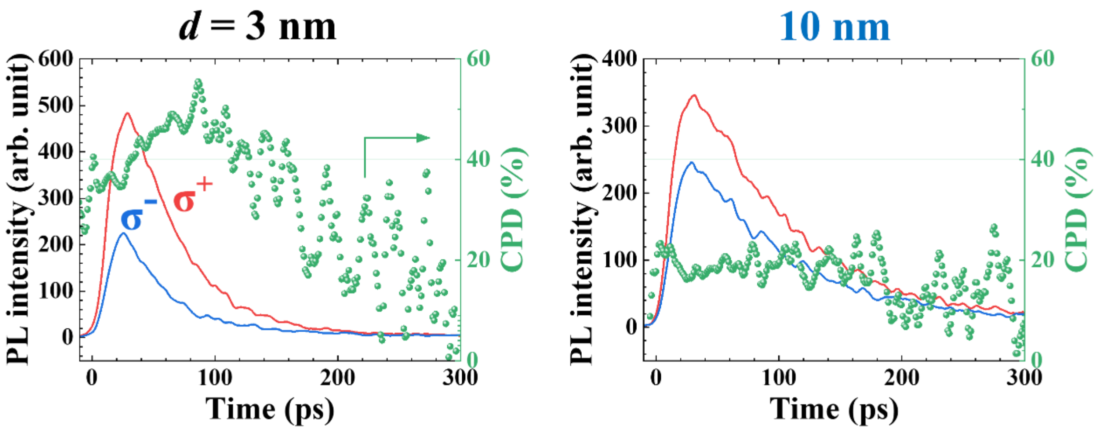

Figure 5-4. Time-resolved circularly polarized PL and the corresponding CPD of QDs at room temperature.

The second mechanism involves the selective removal of minority electron spins from the QD (Figure 5-5 (b)). This mechanism may appear similar to the second-step spin filtering described in Chapter 4.2, but it is different because our focus is more on the occupancy density of states than the energy alignment. Localized states in GaNAs selectively capture minority spins of conduction band electrons, allowing minority spins injected from the GaAs barrier to QDs to be selectively transferred to GaNAs through wavefunction coupling. We hypothesize that these two mechanisms contribute to the high CPDof QD luminescence, corresponding to high

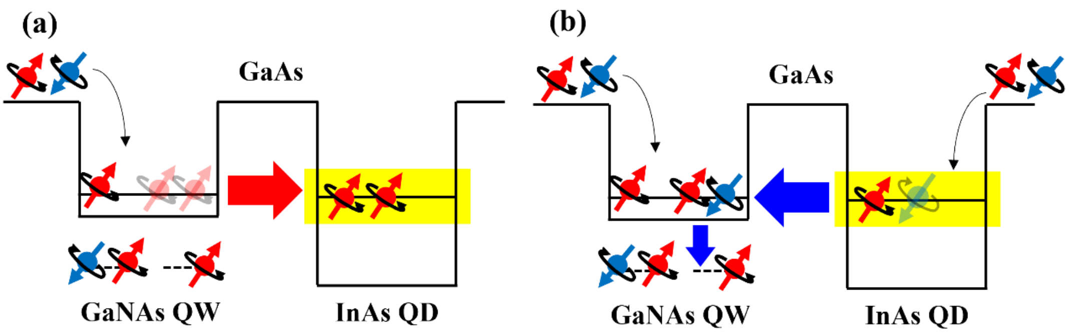

Figure 5-5. Schematic illustrations of spin dynamics. (a) Tunnel injection of highly-polarized electron spins from QW to QD and (b) selective removal of minority electrons spins from QD.

spin polarization at QD states.

5.4 Conclusion

To investigate the effects of various parameters and optimize the sample structure of the GaNAs QW–InAs QDs tunnel-coupled structure, we explored the tunnel-barrier thickness dependence of the optical spin properties of InAs QDs. Two noteworthy features were observed in the electron spin properties of this nanostructure. Firstly, electrons with amplified spin polarization in GaNAs QW were tunnel-injected into QDs. Secondly, minority spins were selectively transferred from QDs to the tunnel-coupled GaNAs QW. Consequently, the InAs QDs tunnel-coupled with GaNAs QW exhibited an enhanced CPD of QD luminescence at ambient temperature. This outcome suggests that, even if energy alignment is not strictly controlled, the remote spin filtering effect of GaNAs QW can influence the optical spin properties of tunnel-coupled QDs.

References

[1] Y. Huang, V. Polojärvi, S. Hiura, P. Höjer, A. Aho, R. Isoaho, T. Hakkarainen, M. Guina, S. Sato, J. Takayama, A. Murayama, I. A. Buyanova and W. M. Chen, Nat. Photonics **9**, 259 (2015).

[2] C. E. Pryor and M. E. Flatte, Phys. Rev. Lett. **96,** 026804 (2006).

[3] D. Lagarde, L. Lombez, X. Marie, A. Balocchi, T. Amand, V. K. Kalevich, A. Shiryaev, E. Ivechenko, and A. Egorov, Phys. Status Solidi A **204**, 208 (2007).

[4] X. J. Wang, I. A. Buyanova, F. Zhao, D. Lagarde, A. Balocchi, X. Marie, C. W. Tu, J. C. Harmand, and W. M. Chen, Nat Mater. **8**, 198 (2009).

Chapter 6. GaNAs QW thickness dependence of optical spin properties of InAs QDs

6.1 Background

In Chapter 5, we established that the tunnel-coupled GaNAs QW significantly influences the optical spin properties of InAs QDs, even in cases where the energy levels were not precisely aligned. Subsequently, in pursuit of optimizing the structure of InAs QD–GaNAs QW, we examined the impact of GaNAs QW thickness on the optical spin properties of InAs QD emission. The findings from this chapter have been published in Applied Physics Letters [1].

6.2 Experimental procedure

6.2.1 Sample structure

Figure 6-1 depicts schematic images of the InAs QD–GaNAs QW tunnel-coupled structure with varying GaNAs QW thicknesses (d = 5, 10, and 20 nm). The GaAs tunnel barrier thicknesses were fixed at 3 nm, and the nominal nitrogen composition was approximately 1% [2]. Assuming the same density of localized states (LS) in GaNAs for all three samples, an increase in the number of LSs is expected with the GaNAs thickness (d) increment. In Figure 6-2 (b, c, d), the band calculation results are presented. The red lines depict the square of the electron and hole wavefunctions of the QD ground state (GS), while the blue lines represent the GS of the GaNAs QW state. These calculations are based on the cross-sectional image obtained from bright-field scanning transmission electron microscopy (STEM) shown in Figure 6-2 (a). The hole wavefunction is localized in the QD GS state, emphasizing that the observed emission mainly originates from the QD state. The energy level of the GaNAs QW changes with variations in QW thickness, thereby altering the energy alignment between the GaNAs QW and QD GS. The insets of Figure 6-2 (b, c, d) illustrate the spatial profile of the existence probability of the electron wave function of the QD GS. These insets suggest differences in spatial coupling, potentially influencing distinct optical spin properties.

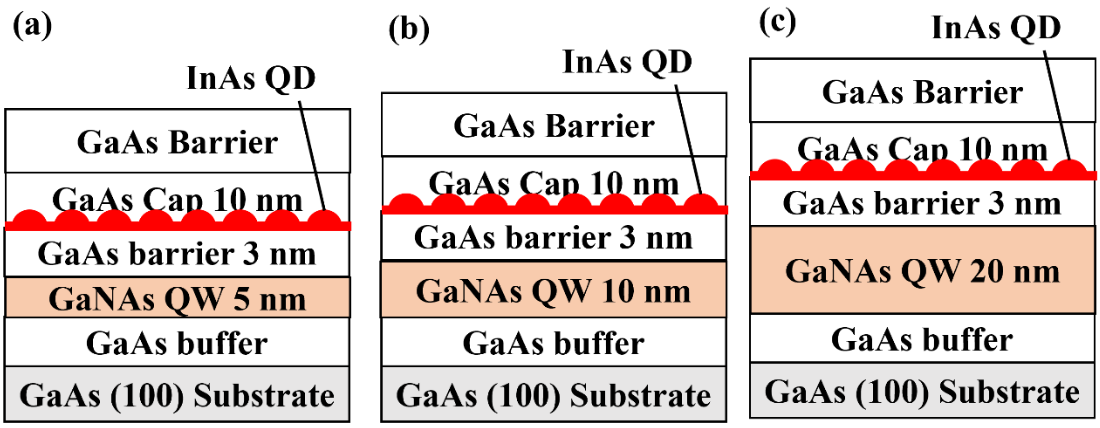

Figure 6-1. Schematic images of InAs QD – GaNAs QW tunnel coupled structure with different GaNAs QW thicknesses.

6.2.2 PL measurement

Circularly polarized time-resolved PL was measured at ambient temperature using a near-infrared (NIR) streak camera. Simultaneously, spin-independent PL spectra were measured using an infrared (IR) camera, known for its heightened sensitivity to lower energy emissions. The excitation energy was adjusted to generate spin-polarized carriers in the GaAs barriers.

6.3 Results and discussion

6.3.1 PL spectra

Figure 6-3 displays the normalized PL spectra of each sample measured with low excitation power at ambient temperature. All four samples exhibit a common peak around 1.08 eV, indicating the successful creation of an identical QD structure. Furthermore, the samples with GaNAs QW feature peaks on the higher-energy side, while the reference QD sample shows only one peak. This observation suggests that the peak at 1.08 eV originates from QD emissive states, while the higher-energy peaks arise from the GaNAs QW states [2].

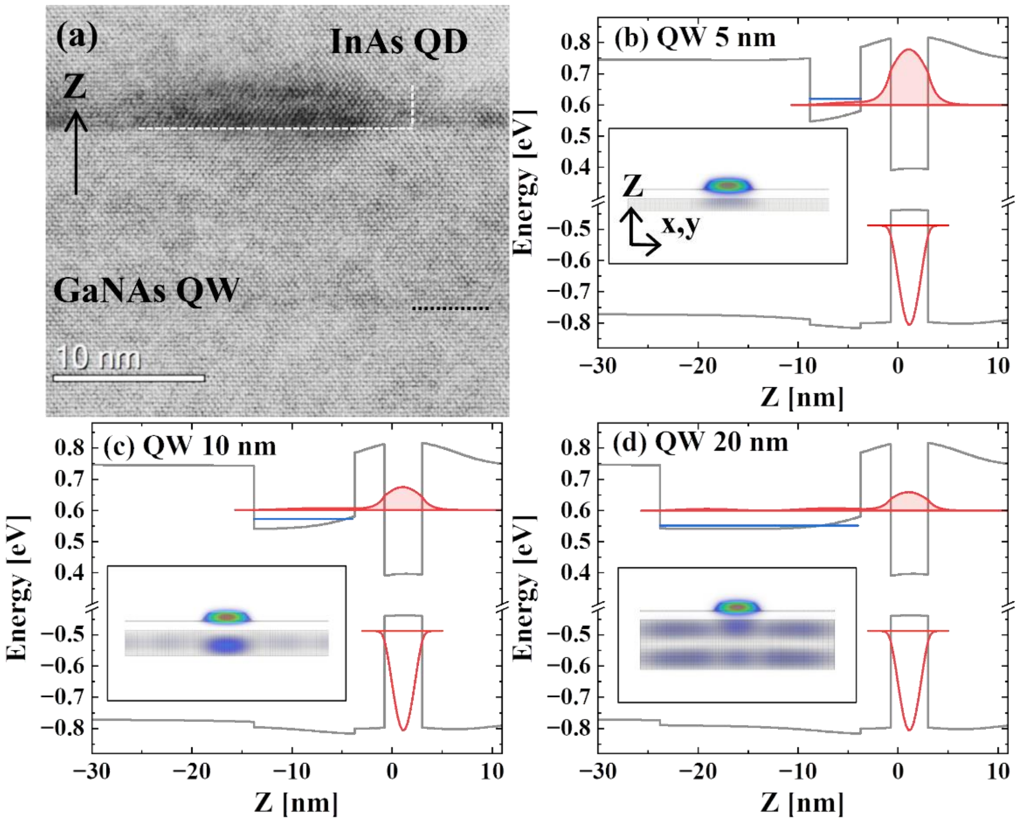

Figure 6-2. Cross-sectional image of bright-field scanning transmission electron microscopy (STEM) of d = 10 nm sample. (b,c,d) Band calculation results. Red lines show the square of the electron and hole wave function of QD GS and clue lines show the GS of GaNAs QW state. Insets are the spatial profile of the existence probability of electron wave function of QD GS.

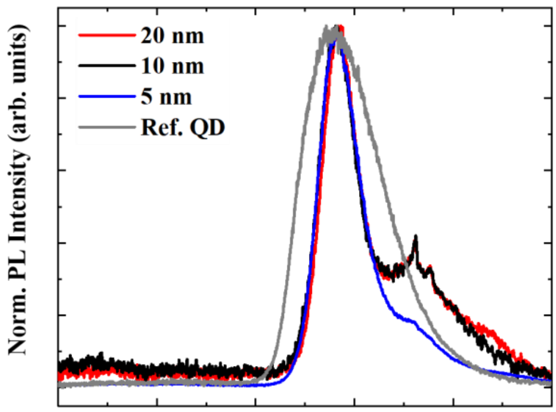

Figure 6-3. Normalized PL spectra of each sample measured with low excitation at room temperature.

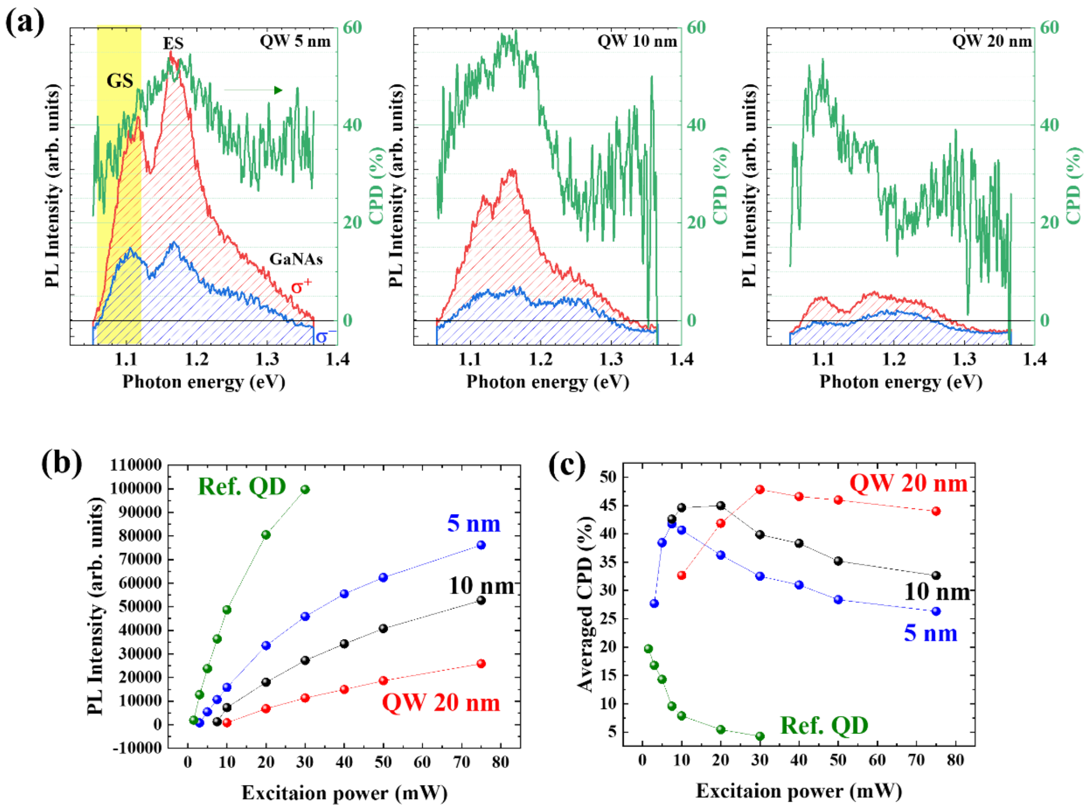

Figure 6-4. (a) Circularly polarized PL spectra and the corresponding CPDs (a green line) for GaNAs QW–InAs QD tunnel-coupled structures. Sum of the PL intensity of QD GS (b) and the averaged CPD (c) as a function of excitation power.

Subsequently, we conducted circularly polarized PL measurements, and the results are depicted in Figure 6-4 (a). The yellow rectangle in the circularly polarized PL spectra of the d = 5-nm sample represents the QD ground state (GS). Figure 6-4 (b) illustrates the sum of the PL intensity of the QD GS as a function of excitation power. The PL intensity decreases with increasing GaNAs QW thicknesses. This reduction in PL intensity is attributed to the capture of a larger number of carriers by LSs in GaNAs [3]. As mentioned earlier, a thicker GaNAs QW implies a greater number of LSs in the GaNAs layer. Consequently, the increased LSs lead to more carriers being captured, resulting in a weaker PL intensity. This outcome indicates that the InAs QD states of all samples with GaNAs QW are effectively influenced by the GaNAs QW, as evidenced by the lower PL intensity compared to that of the reference QD sample.

Figure 6-4 (c) presents the averaged CPD of the QD GS as a function of excitation power. The averaged CPD of the reference QD (depicted by green circles and lines in Figure 6-4(c)) sharply decreases due to the spin-dependent state-filling effect [4, 5]. In contrast, the samples with GaNAs QW exhibit a notably high CPD compared to the reference QD sample, attributed to the spin-filtering effect of the tunnel-coupled GaNAs [6, 7, 8]. However, the averaged CPD reaches its maximum at different excitation powers, and the values vary slightly.

6.3.2 Time-resolved PL

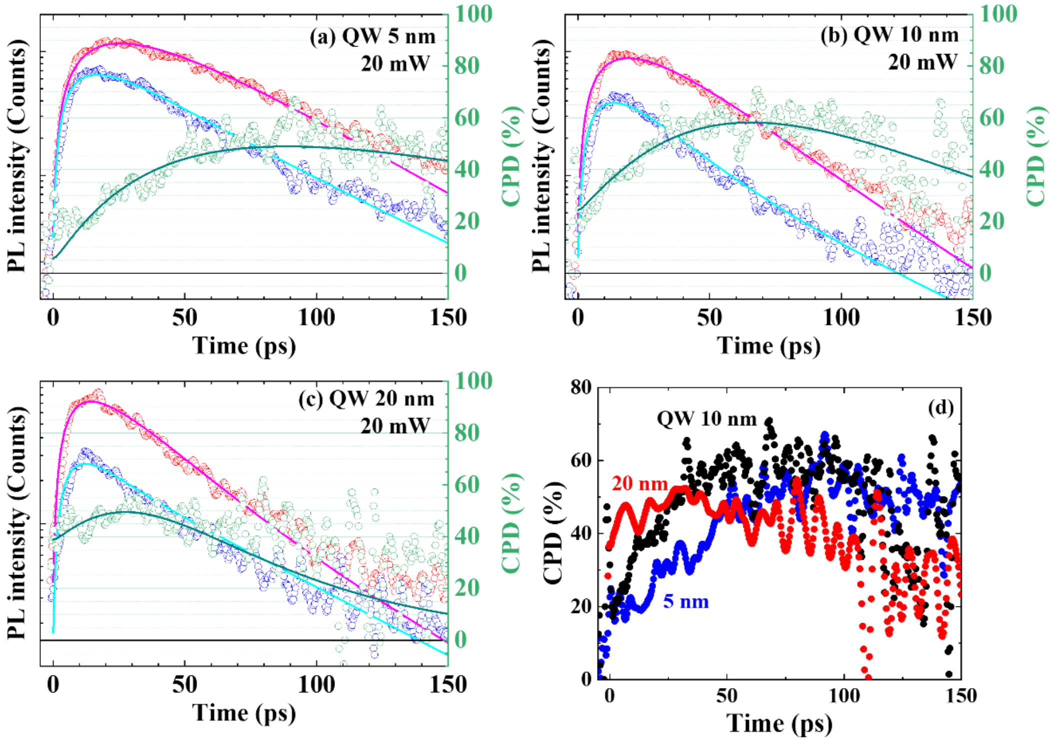

Figure 6-5. Circularly polarized transient RT PL and corresponding CPDs of QD GS for (a) $d = 5$ nm, (b) 10 nm and (c) 20 nm samples, with excitation power of 20 mW. Solid lines depict best-fitted results of rate equation for transient PL and CPD. (d) Time-transient CPD of $d = 5$, 10 and 20 nm samples.

Figures 6-5 (a, b, c) depict the time-transient circularly polarized PL and corresponding CPDs of the QD GS (highlighted with a yellow rectangle in Figure 6-4(a)) at ambient temperature. The solid lines represent the best-fitted results of the rate equation described in Chapter 3.3 for the transient PL and CPD. In Figure 6-5(d), noticeable differences are observed in the initial CPD value, CPD rise, and CPD decay time.

The sample with $d = 5$ nm exhibits a low initial CPD of 20%, and the CPD rise time, indicating the time for CPD to reach its maximum, is the slowest, with a value of about 90 ps. However, after the gradual CPD amplification, the enhanced CPD is maintained for an additional 50 ps. For the $d = 10$-nm sample, an initial CPD of 20%

is observed with a relatively slow CPD rise of 70 ps. Notably, the CPD reaches a maximum of higher than 60%, the highest among the three samples. The *d* = 20-nm sample displays the highest initial CPD of 40% and the fastest CPD rise; however, the CPD rapidly decays after the rapid amplification. Additionally, the *d* = 10- and 20-nm samples demonstrate a faster PL decay than the *d* = 5-nm sample. These characteristics reflect differences in the dominant spin amplification dynamics of the QDs among the three samples. The initial CPD and CPD rise time are susceptible to the spin amplification degree of the GaNAs QWs and the injection speed of spin-amplified electrons. However, as the GaAs barrier is photoexcited in this case, the QD PL encompasses contributions from electron spins directly injected from the GaAs barrier, in addition to those from the GaNAs QWs. In the following discussion, we characterize the characteristic spin amplification dynamics of the QDs.

The features of the *d* = 5-nm sample are a low initial CPD, a gradual CPD rise, and a long duration of the high CPD. As shown in Figure 6-2 (b), the electron wavefunction coupling between the QW and QD is relatively weak for the *d* = 5-nm sample. This weak coupling causes a slow spin injection from the QW to QDs, indicating that the contribution of GaNAs spin filtering to the initial CPD should be small, as reflected in the lowest a_{QW} value listed in Table 1. Thus, the initial CPD is mainly affected by the depolarized electron spins directly injected from the GaAs barrier. However, the contribution of GaNAs sin filtering to the CPD properties should be dominant in the second-half time range (Figure 6-5(a)). Because minority electron spins are selectively removed from the QDs, τ_{c-} is significantly faster than τ_{c+}, resulting in the *d* = 5-nm sample exhibiting the longest τ_{c+}. The extended τ_{c+} indicates a minimal capture rate of majority electron spins by the LSs, i.e., the highest occupancy of the LSs. This outcome is mainly attributed to the smallest number of the LSs in the thinnest QW. Furthermore, the number of effective LSs affecting the QD PL should be small because the QD electron wavefunctions penetrated the QW are limited in the small area just below the QD (Figure 6-2 (b)). These two factors can effectively increase the occupancy of the LSs by majority spins, leading to the longest τ_{c+}. The resulting slow τ_{c+}—significantly longer than τ_{c-}—can suppress the CPD decay, as simulated in Figure 3-6(c).

Table 6-1. Best fitted parameters for *d* = 5, 10 and 20 nm samples.

QW thickness (nm)	$\boldsymbol{\tau_{c+}(\tau_{c-})}$ **(ps)**	$\boldsymbol{a_{QW}}$	$\boldsymbol{\tau_{inj}^{QW}}$ **(ps)**	$\boldsymbol{N_{QW}/N_b}$
5	220 (11)	0.53	21	4
10	81 (13)	0.62	14	9
20	55 (11)	0.71	8	3

For the *d* = 20-nm sample, the electron wavefunction coupling between the QW and QD is stronger than that for the *d* = 5-nm sample (Figure 6-2). This strong coupling causes the fast spin injection from the QW to QDs, i.e., the faster τ_{inj}^{QW} of 8 ps (Table 6-1). We anticipate that the fast injection of spin-amplified electrons in QW can increase the contribution of the GaNAs LSs to the QD PL, leading to not only an increase in a_{QW} but also a decrease in τ_{c+}. In this case, both the majority and minority spins will likely be removed from the QDs (Figure 6-6(b)), resulting in a rapid CPD decay in addition to the fast PL decay.

For the *d* = 10-nm sample, the highest N_{QW}/N_b of 9 was obtained, indicating that the large amount of QD PL originated from the spin-amplified electrons injected from the GaNAs QW. Due to the smaller energy difference between QD GS and QW GS for the *d* = 10-nm sample than the *d* = 20-nm sample, the strongest wavefunction coupling between the QW and QD was observed (Figure6-2 (b)). This coupling can enhance the contribution of the GaNAs spin filtering to the QD PL, thereby yielding the highest CPD value.

6.3.3 PL intensity dependence

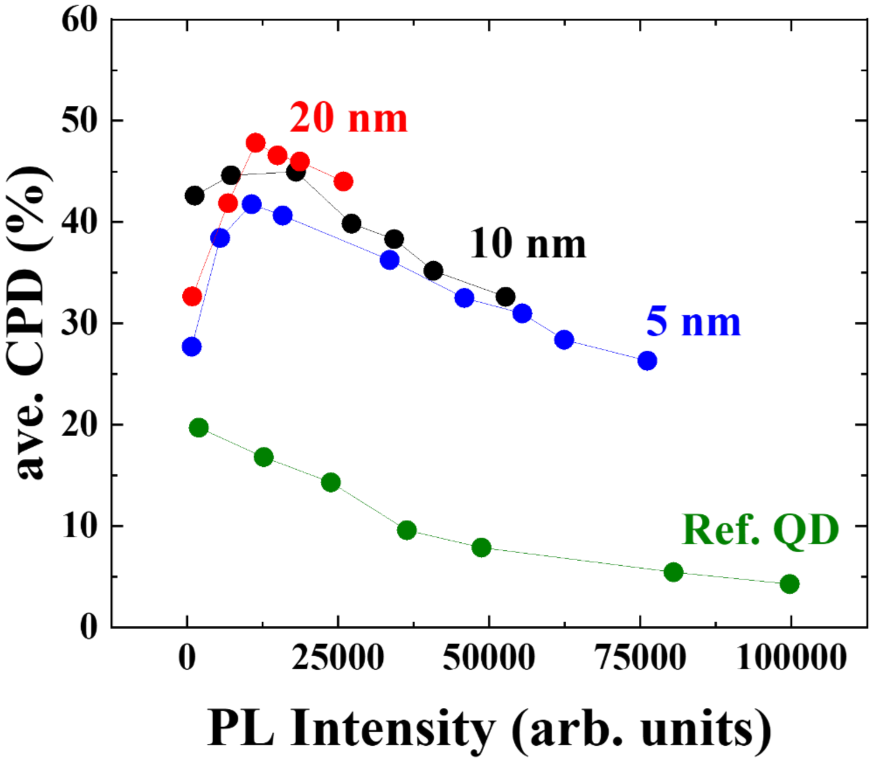

Figure 6-6. Averaged CPD of the PL from QD GS as a function of PL intensity.

Towards the conclusion of section 6.3, an additional intriguing result is presented in Figure 6-6, illustrating the averaged CPD of the PL from QD GS relative to PL intensity. This plot suggests that all three samples with GaNAs QW reach maximum CPD at nearly the same PL intensity. While further analysis is required to definitively ascertain whether this is coincidental, it is plausible that manipulating the excitation power could yield PL of comparable intensity and CPD values. It is essential to underscore, however, that the electron spin dynamics vary with the GaNAs QW thickness, as elucidated in the preceding chapter.

6.4 Conclusion

In this investigation, we explored the influence of GaNAs QW thickness on the dynamics of spin amplification in tunnel-coupled InAs QDs. The rate equation fitting of circularly polarized PL and corresponding CPD unveiled that the spin amplification effect in the GaNAs QW and the spin injection dynamics into the QDs were contingent on the QW thickness. With a QW thickness of 5 nm, the temporal CPD amplification was gradual due to weak wavefunction coupling between the QW and QD. However, a prolonged high CPD was sustained, facilitated by the restrained capture of QD majority spins, originating from the limited number of effective LSs, relative to the efficient removal of QD minority spins. In the case of the 20-nm-thick QW, robust spin filtering in GaNAs and intense wavefunction coupling induced swift CPD amplification with a high initial CPD. Nonetheless, the CPD swiftly diminished post-amplification, attributed to the capture of both QD majority and minority spins. These outcomes offer a straightforward approach to fine-tune ambient temperature spin amplification in QDs by adjusting the thickness of the tunnel-coupled GaNAs QW.

References

[1] Shino Sato, Satoshi Hiura, Junichi Takayama, and Akihiro Murayama, Applied Physics Letters **123**, 232405 (2023).

[2] I. Vurgaftman and J. R. Meyer, J. Appl. Phys. **94**, 3675 (2003).

[3] A. Nishikawa, Y. G. Hong, and C. W. Tu, J. Vac. Sci. Technol. B **22**, 1515 (2004).

[4] S. Grosse, J. H. H. Sandmann, G. von Plessen, J. Feldmann, H. Lipasnen, M. Sopanen, J. Tulkki, and J. Ahopelto, Phys. Rev. B **55**, 4473 (1997),

[5] S. Hiura, K. Takeishi, M. Urabe, K. Itabashi, J. Takayama, T. Kiba, K. Sueoka, and A. Murayama, Appl. Phys. Lett. **113**, 023104 (2018).

[6] Y. Huang, V. Polojarvi, S. Hiura, P. Hojer, A. Aho, R. Isoaho, T. Hakkarainen, M. Guina, S. Sato, J. Takayama, A. Murayama, I. A. Buyanova, and W. M. Chen, Nat. Photonics **15**, 475 (2021).

[7] D. Lagarde, L. Lombez, X. Marie, A. Balocchi, T. Amand, V. K. Kalevich, A. Shiryaev, E. Ivchenko, and A. Egorov, Phys. Stat. Sol. (a) **204**, 208 (2007).

[8] X. J. Wang, I. A. Buyanova, F. Zhao, D. Lagarde, A. Balocchi, X. Marie, C. W. Tu, J. C. Harmand, and W. M. Chen, Nat. Mater, **8**, 198 (2009).

Chapter 7. GaNAs QW position dependence of optical spin properties of InAs QDs

7.1 Background

Building upon the findings in Chapter 5 [1] and Chapter 6 [2], it is unequivocal that the remote spin filtering effect of GaNAs QWs proves efficacious in attaining elevated CPD from QD emission at ambient temperature. Consequently, in a seamless transition from Chapter 6, our attention shifted towards the spatial alignment of the GaNAs QW layer concerning the InAs QD layer, aiming to identify the optimal GaNAs QW–InAs QD tunnel-coupled structure.

7.2 Experimental procedure

Figure 7-1 illustrates the schematic images of the examined InAs QD–GaNAs QW tunnel-coupled samples, where the relative position of the GaNAs QW is altered—either positioned below, above, or on both sides of the InAs QD layer. Throughout this chapter, we refer to each sample as the "lower QW sample," "upper QW sample," and "both QW sample," respectively. The nominal N concentration in GaNAs is approximately 1%. The growth conditions remain consistent for each sample, except for the placement of the GaNAs QW. Maintaining a fixed total GaNAs thickness of 10 nm ensures an equivalent number of LSs in GaNAs.

Circularly polarized time-resolved PL measurements were conducted at ambient temperature using a NIR streak camera. The excitation energy was adjusted to generate spin-polarized carriers in the GaAs barriers. According to the optical selection rule [3], the initial spin polarization degree of the generated electrons is 50%.

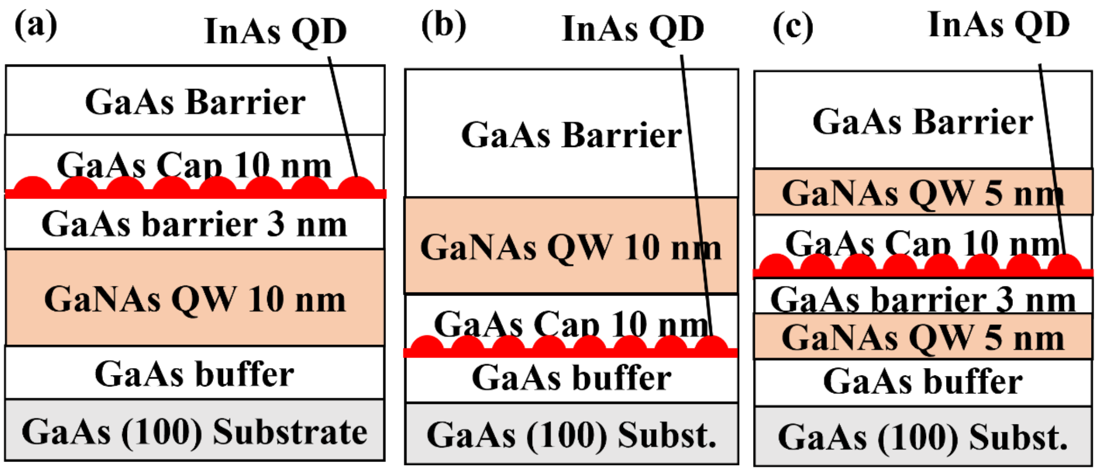

Figure 7-1. Schematic images of InAs QD – GaNAs QW tunnel-coupled structure, whose QW layer exist (a) lower side, (b) upper side and (c) both sides of the QD layer.

7.3 Results and discussion

7.3.1 Circularly polarized PL spectra

Figure 7-2 displays the circularly polarized PL spectra and the corresponding CPDs for each sample at ambient temperature. To enhance clarity, the PL intensities of the both side QW sample [Figure 7-2(c)] have been multiplied by 4.

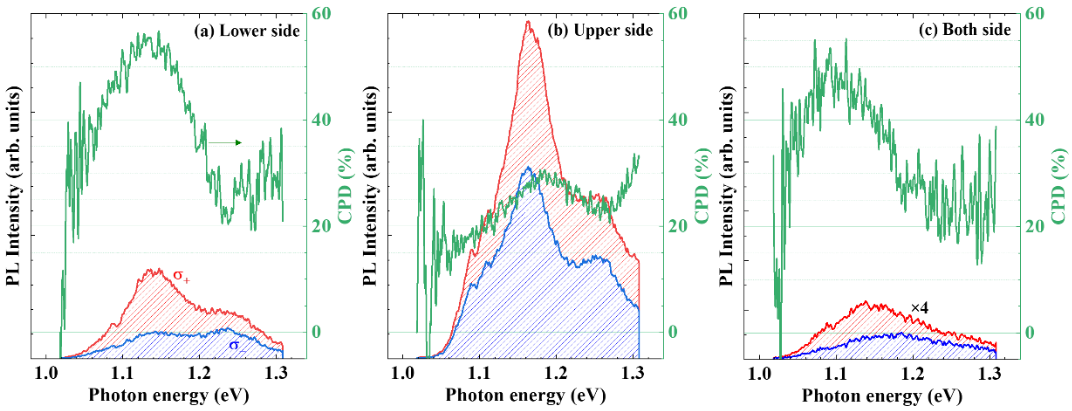

Figure 7-2. Circularly polarized PL spectra and the corresponding CPDs (green lines) for GaNAs QW–InAs QD tunnel-coupled structures, whose QW exists at (a) lower, (b) upper and (c) both side of QD layer. The PL intensities of both side QW sample [Figure 7-2(c)] has been multiplied by 4 for clarity.

Despite the consistent QW thickness of 10 nm, variations in PL intensity are evident among the samples. Specifically, the lower side QW sample and both side QW sample [Figures 7-2(a) and (c)] exhibit weaker PL intensity compared to the upper side QW sample. Additionally, the lower QW sample and both QW sample show higher CPD than the upper QW sample at the lower photon energy side. In other words, the sample without the lower side QW (upper side QW sample) displays stronger PL intensity and lower CPD than the sample with the lower side QW (lower side QW sample and both side QW sample). These findings suggest that the QWs located on the lower side and upper side of the QD have distinct effects on the optical spin properties of the QD.

7.3.2 Excitation power dependence

Figure 7-3 illustrates the excitation power dependencies of the sum of the PL intensity and the averaged CPD of the QD GS. These plots reveal a decreasing trend in PL intensity in the both QW sample, lower QW sample, and upper QW sample, in that order. Conversely, the CPD demonstrates an increasing trend in the same order. Both the reduction in PL intensity and the elevation in CPD are recognized effects of the remote spin filtering effects in GaNAs [4, 5]. Consequently, these two characteristics suggest that the remote spin filtering effect of GaNAs exerts a more significant influence on the both QW sample, followed by the lower QW sample and the upper QW sample. This discrepancy may arise from differences in the probability of tunnel transfer of electron spins between GaNAs QW and InAs QD for each sample, as schematically depicted in Figure 7-4.

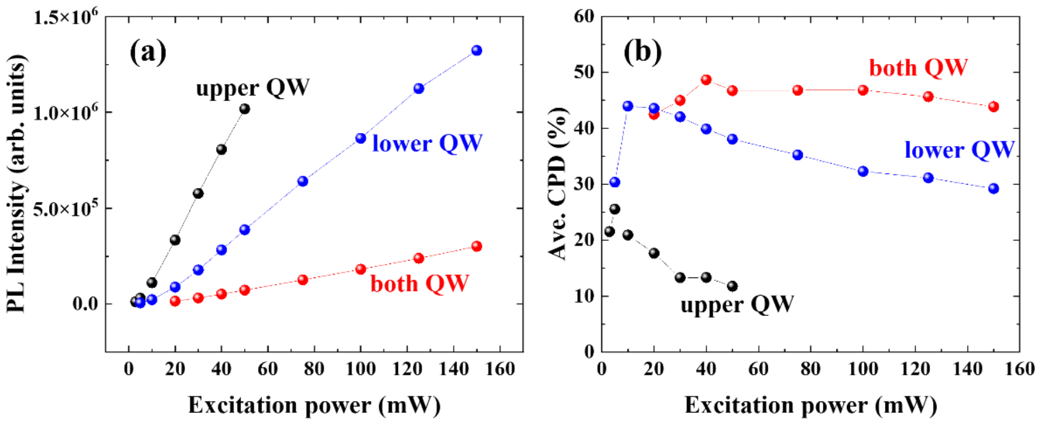

Figure 7-3. Sum of the PL intensity and (b) averaged CPD of QD GS as a function of excitation power.

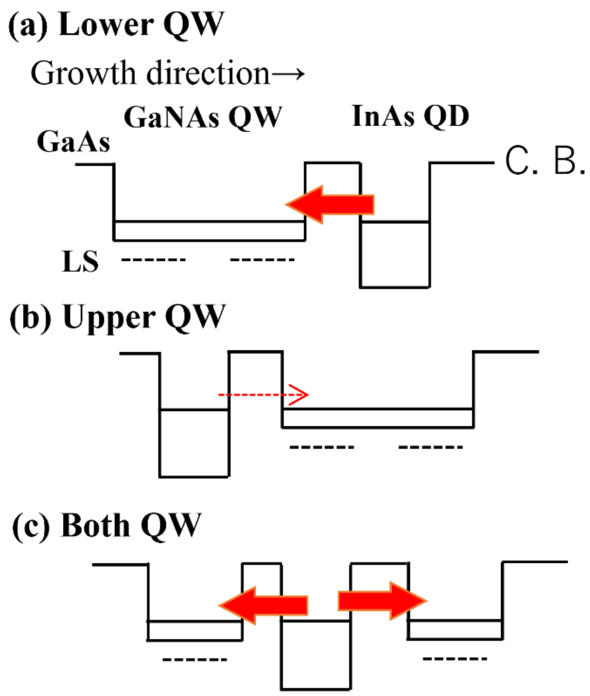

Figure 7-4. Schematic model of electron spin dynamics for (a) lower QW sample, (b) upper QW sample and (c) both QW sample. Red arrows mean the tunnel transfer of electron spins and its thickness mean the probability of tunnel transfer.

7.3.3 Time-resolved circularly polarized PL

In Figure 7-5(a), time-dependent normalized PL intensities are depicted. Notably, only the upper QW sample exhibits a slow PL decay, while the other two samples display faster PL decay. Given that accelerated PL decay has been reported in the context of QD tunnel-coupled with GaNAs [3], this outcome suggests that, in the case of the sample with the lower side QW (lower side QW sample and both side QW sample), InAs QD GSs strongly couple with GaNAs QW.

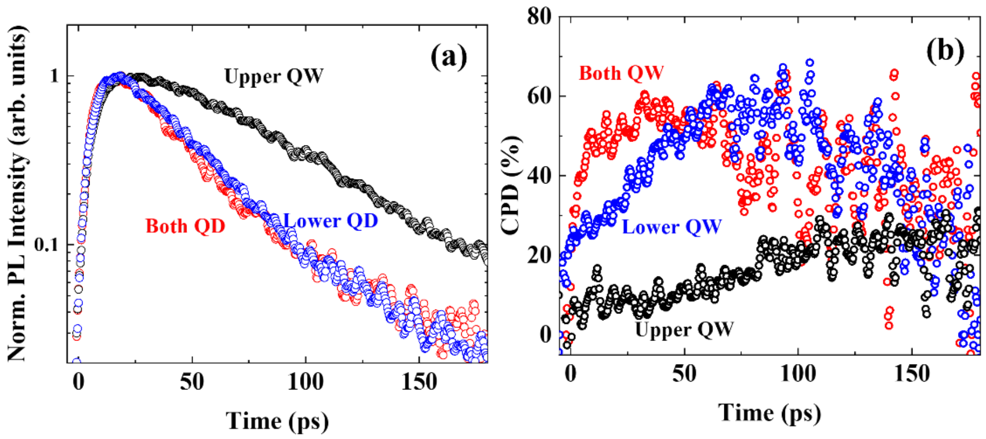

Figure 7-5. Room temperature time-dependent normalized PL intensities (a) and CPD values (b) of QD GS.

In Figure 7-5(b), time-dependent CPD values from the GS of QDs are presented for each sample at ambient temperature. Upon comparing the time it takes for the CPD value to reach its maximum value (CPD amplification time), it is observed that the amplification is faster for the both QW sample, followed by the lower QW sample, and then the upper QW sample.

As discussed in Chapter 2.1.2, the amplification of CPD through GaNAs remote spin filtering effect is attributed to the selective removal of minority electron spins from the QDs to the GaNAs QW and the reinjection of majority electron spins from the QW to the QD (illustrated schematically in Figure 7-6). The observed rapid amplification in both QW samples suggests that these two electron spin dynamics are particularly effective among the three samples.

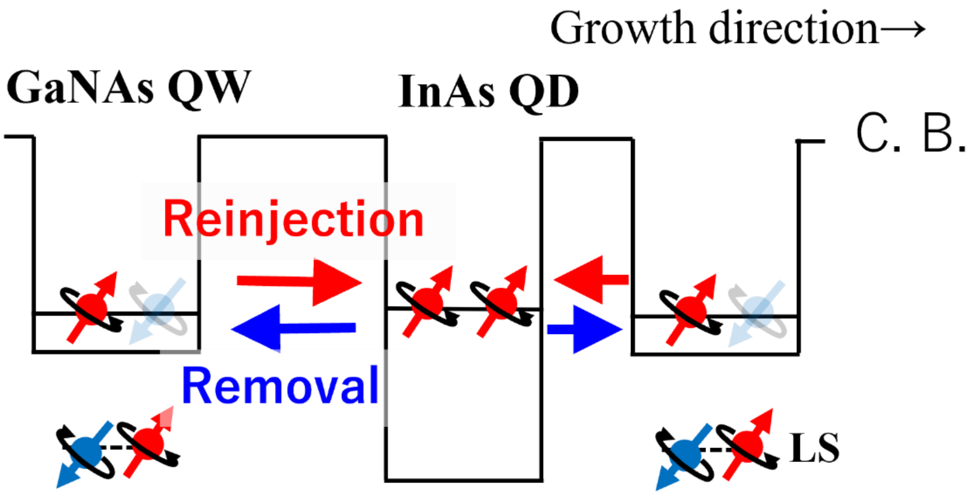

Figure 7-6. Schematic model of remote spin filtering of GaNAs at both QW sample. Red arrows mean reinjection of majority electron spins and blue arrows mean removal of minority electron spins.

In exploring the influence of the relative position of the GaNAs Quantum Well (QW) layer to the InAs Quantum Dot (QD) layer, we systematically investigated three distinct samples: lower QW sample, upper QW sample, and both QW sample, and compared their optical spin dynamics.

The optical spin properties exhibit significant distinctions based on the presence or absence of a lower side QW in the sample. The remote spin filtering effects of GaNAs, including the reduction in Photoluminescence (PL) intensity and the amplification of Circularly Polarized Degree (CPD), are most pronounced in both QW sample, followed by lower QW sample and upper QW sample, in that order. Moreover, through time-resolved circularly polarized PL, the both QW sample demonstrates the highest averaged CPD, attributed to a combination of decreased PL decay time and rapid CPD amplification.

This study highlights that, alongside QW thickness and nitrogen composition in GaNAs, previously explored as parameters for GaNAs, the position of the GaNAs QW layer plays a crucial role in controlling the optical spin properties of tunnel-coupled Quantum Dots (QDs).In exploring the influence of the relative position of the GaNAs QW layer to the InAs QD layer, we systematically investigated three distinct samples: lower QW sample, upper QW sample, and both QW sample, and compared their optical spin dynamics.

The optical spin properties exhibit significant distinctions based on the presence or absence of a lower side QW in the sample. The remote spin filtering effects of GaNAs, including the reduction in PL intensity and the amplification of CPD, are most pronounced in both QW sample, followed by lower QW sample and upper QW sample, in that order. Moreover, through time-resolved circularly polarized PL, the both QW sample demonstrates the highest averaged CPD, attributed to a combination of decreased PL decay time and rapid CPD amplification.

This study highlights that, alongside QW thickness and nitrogen composition in GaNAs, previously explored as parameters for GaNAs, the position of the GaNAs QW layer plays a crucial role in controlling the optical spin properties of tunnel-coupled QDs.

References

[1] Y. Huang, V. Polojärvi, S. Hiura, P. Höjer, A. Aho, R. Isoaho, T. Hakkarainen, M. Guina, S. Sato, J. Takayama, A. Murayama, I. A. Buyanova and W. M. Chen, Nat. Photonics **9**, 259 (2015).

[2] Shino Sato, Satoshi Hiura, Junichi Takayama, and Akihiro Murayama, Applied Physics Letters **123**, 232405 (2023).

[3] F. Meier, and B. Zakharchenya, Optical Orientation, (Elsevier, North-Holland, Amsterdam, 1984).

[4] D. Lagarde, L. Lombez, X. Marie, A. Balocchi, T. Amand, V. K. Kalevich, A. Shiryaev, E. Ivechenko, and A. Egorov, Phys. Status Solidi A **204**, 208 (2007).

[5] X. J. Wang, I. A. Buyanova, F. Zhao, D. Lagarde, A. Balocchi, X. Marie, C. W. Tu, J. C. Harmand, and W. M. Chen, Nat Mater. **8**, 198 (2009).

Chapter 8. Conclusion

In this investigation, the primary goal involved achieving both high luminosity and elevated circular polarization emission in QDs by leveraging the unique properties of GaNAs. This material has been previously reported to exhibit high luminescence circular polarization at ambient temperature, accompanied by heightened circular polarization of the luminescence, indicative of enhanced electron spin polarization. However, due to the entrapment of numerous carriers in localized levels, leading to a reduction in luminescence intensity, it becomes imperative to optimize the quantum structure. Consequently, this study involves the fabrication of samples featuring varying thicknesses and arrangements of GaNAs QWs and GaAs tunnel barriers. The overarching objective is to derive design guidelines for quantum structures with the aim of optimizing the trade-off between luminosity and circular polarization in QDs.

In Chapter 5, the investigation into GaNAs QW-InAs QD tunnel-coupled nanostructures commenced by studying samples with varying GaAs tunnel barrier thicknesses. In instances where a thin tunnel barrier was employed, the luminescence intensity of QD decreased, while the circular polarization of luminescence increased. This phenomenon is attributed to the enhanced coupling between the QW and QD electronic wavefunctions, which becomes more pronounced with decreasing tunnel barrier thickness. The study emphasizes the prominent role of GaNAs in influencing the circularly polarized luminescence properties of QDs. In this research, InAs QDs were fabricated atop 20 nm GaNAs QWs. Contrary to expectations, thin tunnel barriers did not adversely affect the QD structure grown on top, showing no discernible impact on the GaNAs layer distortion. Surprisingly, there was no observable difference in the QD structure based on tunnel barrier thickness. As a result, for subsequent discussions in Chapters 6 and 7, the tunnel barrier thickness remained fixed at 3 nm. This consistent parameter choice facilitates a more focused exploration of the interplay between QW and QD in the ensuing chapters.

In Chapter 6, the investigation delved into the influence of GaNAs QW film thickness on the circularly polarized emission characteristics of InAs QDs through time-resolved circularly polarized light PL. The temporal variation of circular polarizability was found to be contingent on the GaNAs QW film thickness. The electron spin dynamics were modeled using a rate equation that considered electron spin transfer between GaNAs QWs and InAs QDs, along with the spin capture of localized levels in GaNAs. In the sample with the thinnest QW film (5 nm), the spin-capture time of GaNAs localized levels exhibited significant variability based on spin direction. A swift transfer of spins from QDs to GaNAs localized levels, coupled with a substantial remaining spin population in the QDs, led to a prolonged maintenance of amplified circular polarization during emission. However, the limited number of localized levels contributing to QD luminescence resulted in a small circular polarization amplification time. Moving to the sample with a medium QW film thickness (10 nm), the amplification time surpassed that of the sample with a thinner QW film. The close energetic alignment of GaNAs QW levels and InAs QD levels facilitated easy electron spin transfer between them, intensifying the circular polarization of QDs. Consequently, GaNAs exerted a stronger influence on the circularly polarized luminescence properties of QDs, culminating in the highest achievable circular polarization. Finally, in the sample with the thickest QW film (20 nm), the amplification of spin polarization at the QW, coupled with rapid spin injection from QW to QD, resulted in swift circular polarizability amplification. This observation emphasizes the intricate interplay between QW film thickness and spin dynamics, shedding light on the nuanced factors impacting circular polarization in QD emission.

In Chapter 7, I explored the impact of GaNAs QW arrangement on the circularly polarized luminescence properties of QDs by altering the positioning of GaNAs QWs. Previously situated at the bottom of the QDs, three sample types were fabricated with QWs at the top, bottom, and both top and bottom. A comparative analysis between samples with QWs at the bottom and those with QWs at the top revealed an enhancement in the circularly polarized emission characteristics of QDs when QWs were positioned at the bottom, despite maintaining the same QW thickness. Moreover, the examination unveiled that the sample with QWs at both the top and bottom exhibited a more pronounced influence from GaNAs compared to the sample with QWs only at the bottom. Notably, this outcome cannot be solely explained by aggregating the effects of lower and upper QWs, suggesting a potential connection to the intricate coupling state of electronic wavefunctions arising from the placement of QWs at both ends of the QD.

In conclusion, this study has revealed a substantial transformation in the electron spin dynamics within tunnel-coupled nanostructures of GaNAs QWs and InAs QDs by altering film thickness configuration and arrangement. Notably, adjusting the thickness of GaNAs QWs not only impacts the strength of the GaNAs spin amplification effect but also alters the spin injection time into the QDs. These findings offer valuable insights for designing quantum structures aimed at achieving high-speed spin amplification, a crucial requirement for the high-frequency operation of spin-emitting devices.

Research achievements

Publications

[1] Satoshi Hiura, Mizuki Takisita, Junichi Takayama, Shino Sato, and Akihiro Murayama:

「Highly efficient room-temperature electron-photon spin conversion using semiconductor

hybrid nanosystem with gradual quantum dimensionality reduction」, Physical Review

Applied 14, 044011 (2020). (IF = 4.931)

[2] Shino Sato, Satoshi Hiura, Junichi Takayama, and Akihiro Murayama: 「Suppression of

thermally excited electron-spin relaxation in InGaAs quantum dots using p-doped capping

layers toward enhanced room-temperature spin polarization」, Applied Physics Letters,

116, 182401 (2020).

[3] Shino Sato, Satoshi Hiura, Junichi Takayama, and Akihiro Murayama: 「Temperature dependence of inter-dot electron-spin transfer among laterally coupled excited states in highdensity InGaAs quantum dots」, Journal of Applied Physics **127**, 4, 043904 (2020).

[4] Yuqing Huang, Ville Polojärvi, Satoshi Hiura, Pontus Höjer, Arto Aho, Riku Isoaho, Teemu Hakkarainen, Mircea Guina, Shino Sato, Junichi Takayama, Akihiro Murayama, Irina A. Buyanova, and Weimin M. Chen:「Room-temperature electron spin polarization exceeding 90% in an opto-spintronic semiconductor nanostructure via remote spin filtering」, Nature Photonics **15**, 475 (2021).

[5] Keisuke Minehisa, Ryo Murakami, Hidetoshi Hashimoto, Kaito Nakama, Kenta Sakaguchi, Rikuo Tsutsumi, Takeru Tanigawa, Mitsuki Yukimune, Kazuki Nagashima, Takeshi Yanagida, Shino Sato, Satoshi Hiura, Akihiro Murayama , and Fumitaro Ishikawa:「Wafer-scale integration of GaAs/AlGaAs core-shell nanowires on silicon by the single process of self-catalyzed molecular beam epitaxy」, Nanoscale Advances **5**, 1651 (2023).

[6] Shino Sato, Satoshi Hiura, Junichi Takayama, and Akihiro Murayama:「Effect of dilute

nitride GaNAs quantum well thickness on spin amplification dynamics of tunnel coupled

InAs quantum dots」, Applied Physics Letters **123**, 232405 (2023).

Conferences

International conference

[1] ○Shino Sato, Satoshi Hiura, Junichi Takayama, and Akihiro Murayama:「Temperature dependence of spin dynamics at laterally coupled excited states of InGaAs quantum dots」,2nd JSPS workshop on Japan-Sweden frontiers in photon and spin functionalities of nanomaterials, Noboribetsu, Japan, October 24, P-1, (2018) -poster

[2] ○Shino Sato, Satoshi Hiura, Junichi Takayama, and Akihiro Murayama: 「Temperature Dependence of Interdot Spin Dynamics in Laterally Coupled InGaAs Quantum Dots」, 31st International Microprocesses and Nanotechnology Conference, Sapporo, Japan, Nov. 13-16, 16p-11-64, (2018) -poster

[3] ○Shino Sato, Motoya Murakami, Yuto Nakamura, Satoshi Hiura, Junichi Takayama, and Akihiro Murayama: 「Effects of p-doping on excited spin states and the dynamics in InGaAs quantum dots」,Compound Semiconductor Week 2019, Nara, Japan, May 19-23, MoP-E-9, (2019) -poster

[4] ○Yuto Nakamura, Satoshi Hiura, Shino Sato, Junichi Takayama, Akihiro Murayama: 「Effects of growth temperature of a capping layer on excited spin properties of $In_{0.5}Ga_{0.5}As$ quantum dots」, Compound Semiconductor Week 2019 , Nara, JAPAN, TuP-A-4, May 19-23, (2019) -poster

[5] ○Shino Sato, Satoshi Hiura, Junichi Takayama, and Akihiro Murayama: 「P-doping effects on temperature-dependent spin dynamics in InGaAs quantum dots」, 7th International Workshop on Epitaxial Growth and Fundamental Properties of Semiconductor Nanostructures, Kobe, JAPAN, P-01, Sept. 24-27 (2019) -poster

*Best poster award

[6] ○Yuto Nakamura, Satoshi Hiura, Shino Sato, Junichi Takayama, Akihiro Murayama: 「Temperature-dependent spin dynamics in InGaAs quantum dots embedded with GaAs capping layer grown at low temperature」, 7th International Workshop on Epitaxial Growth and Fundamental Properties of Semiconductor Nanostructures, Kobe, JAPAN, P-05, Sept. 24-27 (2019) -poster

[7] ○Shino Sato, Satoshi Hiura, Junichi Takayama, and Akihiro Murayama: 「Highly efficient electron-photon spin conversion using InGaAs quantum dots with p-doped

capping barrier」, 2020 International Conference on Solid State Devices and Materials, Virtual Conference, K-5-03, Sept. 27-30 (2020) -oral

[8] ○Shino Sato, Yuto Nakamura, Soyoung Park, Satoshi Hiura, Junichi Takayama, and Akihiro Murayama:「Optical spin properties of InAs quantum dots tunnel-coupled with dilute nitride GaNAs」, 2021 International Conference on Solid State Devices and Materials, Virtual Conference, H-4-04, Sept. 6-9 (2021) -oral

[9] ○Shino Sato, Masayoshi Hosoe, Satoshi Hiura, Junichi Takayama, and Akihiro Murayama:「Thickness effects of dilute GaAs nitride quantum wells on optical spin properties of tunnel-coupled InAs quantum dots」, The 22nd International Vacuum Congress, Sapporo, Japan, Sept. 11-16, Tue-J2-5, (2022) -oral

[10] ○Shino Sato, Satoshi Hiura, Junichi Takayama, and Akihiro Murayama:「Room-temperature electron-photon spin conversion based on III-V semiconductor quantum dot」, Opinion Exchange Meeting of Hokkaido University-Hitachi Joint Cooperative Support Program for Education and Research in Hitachi Cambridge Laboratory, Cambridge, United Kingdom, Dec. 1, (2023) -oral

[11] ○Masayoshi Hosoe, Shino Sato, Satoshi Hiura, Junichi Takayama, and Akihiro Murayama:「Room-temperature electron spin transport to InAs quantum dots using a dilute nitride GaNAs/GaAs superlattice barrier」, 36th International Microprocesses and Nanotechnology Conference, Sapporo, Japan, November 14-17, 17P-1-33 (2023) -poster

Domestic conference

[1] ○Shino Sato, Satoshi Hiura, Junichi Takayama, and Akihiro Murayama:「Temperature dependence of spin dynamics at coupled excited states of InGaAs

quantum dots」, 79th JSPS Autumn Meeting 2018, Nagoya, Japan, Sept. 19-21, 21a-PA3-11 (2018) -poster

[2] ○Yuto Nakamura, Shino Sato, Satoshi Hiura, Junichi Takayama, and Akihiro Murayama:「Growth temperature dependence of capping layer in InGaAs quantum dots」, 第 54 回応用物理学会北海道支部/第 15 回日本光学会北海道支部合同学術講演会, Hakodate, Japan, Jan. 5-6 (2019) -oral

[3] ○Shino Sato, Satoshi Hiura, Junichi Takayama, and Akihiro Murayama:「Temperature dependence of interdot spin dynamics at coupled excited states of InGaAs quantum dots」, 第 54 回応用物理学会北海道支部/第 15 回日本光学会北海道支部合同学術講演会, Hakodate, Japan, Jan. 5-6 (2019) -oral

[4] ○Yuto Nakamura, Shino Sato, Satoshi Hiura, Junichi Takayama, and Akihiro Murayama:「Temperature dependence of electron spin dynamics in InGaAs quantum dots capped with GaAs layer grown at low temperature」, 80th JSPS Autumn Meeting 2019, Sapporo, Japan, Sept. 18-21, 18p-B31-12 (2019) -oral

[5] ○Shino Sato, Yuto Nakamura, Satoshi Hiura, Junichi Takayama, and Akihiro Murayama:「Electron spin dynamics at excited states of p-doped InGaAs quantum dots」, 80th JSPS Autumn Meeting 2019, Sapporo, Japan, Sept. 18-21, 20p-E302-10, (2019) -oral

[6] ○Shino Sato, Satoshi Hiura, Junichi Takayama, and Akihiro Murayama:「高密度

InGaAs 量子ドット の励起状態における 電子スピンの熱励起効果」, 第 55 回応用物理学会北海道支部/第 16 回日本光学会北海道支部合同学術講演会, Sapporo, Japan, Jan. 11-12, C-5, (2020) -oral

[7] ○Shino Sato, Satoshi Hiura, Junichi Takayama, and Akihiro Murayama: 「Suppression of thermal spin relaxation of InGaAs quantum dots by p-doping」, 81th JSPS Autumn Meeting 2020, Virtual Conference, Sept. 8-11, 8p-Z08-8, (2020) -oral

*English session award

[8] ○Shino Sato, Yuto Nakamura, Soyoung Park, Satoshi Hiura, Junichi Takayama, and Akihiro Murayama:「Spin dynamics in tunnel-coupled structure of dilute nitride GaAs and InAs quantum dots」, 82th JSPS Autumn Meeting 2021, Virtual Conference, Sept. 10-13 and 21-23, 12p-N303-6, (2021) -oral

[9] ○Shino Sato, Satoshi Hiura, Junichi Takayama, and Akihiro Murayama:「Low-power consumption optical transmission of electron-spin information using semiconductor quantum dots」, ME-MMS-AIT 合同研究会, Virtual Conference, Feb. 18-19, (37)ME, (2021) -oral

*keynote address

[10] ○Shino Sato, Satoshi Hiura, Junichi Takayama, and Akihiro Murayama: 「Electron spin amplification dynamics in a tunnel coupling of dilute nitride GaNAs quantum well and InAs quantum dots; effects of the position of quantum well」, 83th JSPS Autumn Meeting 2022, Sendai, Japan, Sept. 20-23, 20p-C401-3, (2022) -oral

[11] ○Masayoshi Hosoe, Shino Sato, Satoshi Hiura, Junichi Takayama, and Akihiro Murayama:「Circularly polarized light emission properties of InAs quantum dots tunnel-coupled with a dilute nitride GaNAs quantum well with different thicknesses」,83th JSPS Autumn Meeting 2022, Sendai, Japan, Sept. 20-23, 21a-A105-6, (2022) -oral

[12] ○Masayoshi Hosoe, Shino Sato, Satoshi Hiura, Junichi Takayama, and Akihiro Murayama:「Electron spin transport to InAs quantum dots using dilute nitride GaNAs/GaAs superlattice barrier」, 84th JSPS Autumn Meeting 2022, Kumamoto, Japan, Sept. 19-23, 20p-A301-8, (2023) -oral

[13] ○Shino Sato, Masayoshi Hosoe, Satoshi Hiura, Junichi Takayama, and Akihiro Murayama:「Optical spin dynamics of InAs quantum dots tunnel-coupled with dilute nitride GaNAs quantum well with different thicknesses」, 84th JSPS Autumn Meeting 2022, Kumamoto, Japan, Sept. 19-23, 20p-A301-8, (2023) -oral